

# Ca isotope cycling in a forested ecosystem

Chris Holmden<sup>1</sup> and Nicolas Bélanger<sup>2</sup>

Saskatchewan Isotope Laboratory<sup>1</sup>, Department of Geological Sciences, University of Saskatchewan, 114 Science Place, Saskatoon, Saskatchewan, S7N 5E2. [chris.holmden@usask.ca](mailto:chris.holmden@usask.ca).

UER Sciences et technologies<sup>2</sup>, Télusq, Université du Québec à Montréal, 100 Sherbrooke Ouest, Montréal, Québec, H2X 3P2. [belanger.nicolas@telusq.uqam.ca](mailto:belanger.nicolas@telusq.uqam.ca).

## ABSTRACT

Reports of large Ca isotope fractionations between trees and soils prompted this study of a Boreal forest ecosystem near La Ronge, Saskatchewan, to improve understanding of this phenomenon. The results on five tree species (black spruce, trembling aspen, white spruce, jack pine, balsam poplar) confirm that nutrient Ca uptake by plants favors the light isotopes, thus driving residual Ca in plant available soil pools towards enrichment in the heavy isotopes. Substantial within-tree fraction occurs in tissues formed along the transpiration stream, with low  $\delta^{44}\text{Ca}$  values in fine roots (2mm), intermediate values in stemwood, and high values in foliage. Separation factors between different plant tissues are similar between species, but the initial fractionation step in the tips of the fine roots is species specific, and/or sensitive to the local soil environment. Soil water  $\delta^{44}\text{Ca}$  values appear to increase with depth to at least 35 cm below the top of the forest floor, which is close to the deepest level of fine roots. The heavy plant fractionated signature of Ca in the finely rooted upper soils filters downward where it is retained on ion exchange sites, leached into groundwater, and discharged into surface waters.

The relationship between Ca uptake by tree fine roots and the pattern of  $^{44}\text{Ca}$  enrichment with soil depth was modeled for two Ca pools: the forest floor (litter) and the underlying (upper B) mineral soil. Six study plots were investigated along two hillside toposequences trending upwards from a first order stream. We used allometric equations describing the Ca distribution in boreal tree species to calculate weighted average  $\delta^{44}\text{Ca}$  values for the stands in each plot and estimate Ca uptake rates. The  $\delta^{44}\text{Ca}$  value of precipitation was measured, and soil weathering signatures deduced, by acid leaching of lower B mineral soils. Steady state equations were used to derive a set of model Ca fluxes and fractionation factors for each plot. The model reproduces the increase in  $\delta^{44}\text{Ca}$  with depth found in forest floor and upper B soil waters. Transient model runs show that the forest Ca cycle is sensitive to changes in plant Ca uptake rate, such as would occur during ontogeny or disturbance. Accordingly, secular records of  $\delta^{44}\text{Ca}$  in tree ring cellulose have the potential to monitor changes in the forest Ca cycle through time, thus providing a new

tool for evaluating natural and anthropogenic impacts on forest health. Another model run shows that by changing the size of the isotope fractionation factor and adjusting for differences in forest productivity, that the range in Ca isotope fractionation in forested ecosystems reported in the literature, thus far, is reproduced. As a quantitative tool, the Ca cycling model produces a reasonable set of relative Ca fluxes for the La Ronge site, consistent with Environment Canada's measurements for wet deposition in the region and simulated Ca release from soil mineral weathering using the PROFILE model. But the sensitivity of the model is limited by the small range of fractionation observed in this boreal shield setting of ~1‰, which limits accuracy. If the model were applied to a site with a greater range in  $\delta^{44}\text{Ca}$  values among the principal Ca fluxes, it is capable of producing robust and reliable estimations of Ca fluxes that are otherwise difficult to measure in forested ecosystems.

## 1. INTRODUCTION

Biogeochemical cycling of Ca in forest ecosystems causes fractionation of Ca isotopes. The ~4‰ range of fractionation documented, thus far, (Schmitt et al., 2003; Bullen et al., 2004; Wiegand et al., 2005; Holmden and Bélanger, 2006; Perakis et al., 2006; Page et al., 2008; Cenkci Tok et al., 2009) is much larger than the ~1‰ effects associated with biotic (Russell and Papanastassiou, 1978a; Skulan et al., 1997; Zhu and MacDougall, 1998; Gussone et al., 2003; Sime et al., 2005; Steuber and Buhl, 2006; Fantle and DePaolo, 2005; Farkas et al., 2007) and abiotic (Lemarchand et al., 2004; Gussone et al., 2005; Fantle and DePaolo, 2007; Jacobson and Holmden, 2008; Ewing et al., 2008) precipitation of Ca bearing minerals from natural waters, or the small range of Ca isotope fractionation in rocks of the crust and upper mantle of about the same magnitude (DePaolo et al., 2004; Amini et al., 2008). These findings point to vegetation and soils as potentially important sources of isotopically fractionated Ca in the Earth's exogenic Ca cycle.

The uptake of Ca into trees favors the lighter isotopes, which causes the residual Ca in soil exchange pools to accumulate the heavier isotopes. Fractionation of Ca isotopes also occurs

between different tissues in trees. For example, Ca in stemwood is depleted in heavy isotopes compared to foliage, but both are enriched in light isotopes compared to plant available soil pools (Holmden and Bélanger, 2006; Page et al., 2008; Cenki Tok et al., 2009). The underlying physiological mechanisms, the prevalence of species effects, and the range of environmental controls that may influence Ca isotope fractionation in trees are not well known.

To improve our understanding of isotope fractionation effects accompanying Ca cycling in forests, we studied an unpolluted Boreal Shield watershed in northern Saskatchewan that was recently the subject of a Ca apportionment study to trees using  $^{87}\text{Sr}/^{86}\text{Sr}$  as a tracer (Bélanger and Holmden, submitted). Measurements of  $\delta^{44}\text{Ca}$  in foliage, stemwood, and fine roots were performed on 5 tree species typical of this ecosystem, growing on a small hillside watershed with a first order stream. The  $\delta^{44}\text{Ca}$  values in soil solutions, soil extracts, soil leaches, shallow groundwater, granite bedrock, precipitation, and stream waters were also measured, thus, generating a complete survey of  $\delta^{44}\text{Ca}$  variability in a high latitude terrestrial ecosystem. We investigate the factors controlling  $\delta^{44}\text{Ca}$  values in plant available soil pools with the help of a steady state Ca cycling model, and an allometric analysis of the Ca distribution in trees. The model is employed to produce a set of balanced Ca fluxes and plant uptake fractionation factors for six study plots differing in soil texture, soil mineralogy, elevation, and stand composition.

## 2. STUDY SITE AND EXPERIMENTAL DESIGN

### 2.1 Study site and design

The study site is a hillside watershed with a first order stream, located along the southern edge of the Precambrian Shield in north-central Saskatchewan, ~40 km north of the town of La Ronge (55° 6' 0" N, 105° 18' 0" W), and ~400 km north of Saskatoon (Fig. 1). Mean annual air temperature is -0.1°C and precipitation is 484 mm. The forests are black spruce/trembling aspen

stands with subsidiary amounts of jack pine. Dendrochronological analysis of the trees revealed two cohorts: one with an age of 80–90 years on slopes and hilltops, and another with an age of 110–120 years in the flood plain of the stream. The forest has never been harvested, and it is presumed that the ages reflect the last time the forest was destroyed by fire. Burn cycles of ~100 years are typical in this region. In 2006, a major fire burned thousands of hectares of forest near La Ronge, but the area surrounding the studied watershed was left intact (Saskatchewan Environment, 2006).

The study site was broken up into three 75 m<sup>2</sup> circular plots strung along two hillside toposequences. Plots in Toposequence 1 are identified as 1.1, 1.2, and 1.3 (Fig. 2). Plot 1.1 covers the highest parts of the slope, plot 1.2 covers the midslope, and plot 1.3 covers the lowermost slope and riparian zone. Toposequence 2 covers two drainage valleys. Plots identified as 2.2 and 2.3 are from the same hillside, and cover the same range of elevations as Toposequence 1, about 40 m upstream (Fig. 3). Plot 2.1 covers a shallow, bowl-like depression at the top of the hill that gently slopes towards the next valley. It lies about 3 m below the top of Toposequence 1. The middle and upper slopes of Toposequence 1 (where the soils are sandier and better drained) range into mixed wood forests with spruce, trembling aspen, and some jack pine. In areas near the stream where the water table is high throughout the growing season (20 to 40 cm depth), balsam poplar and white spruce are found alongside the dominant black spruce. The forest on Toposequence 2 is uniformly black spruce with a feathermoss understory.

General soil properties are tabulated in Bélanger and Holmden (submitted). Soils under the mixedwood vary from sandy loam to loam in the upper slope areas, and to silt loam in the mid-slope areas. The soils under the black spruce/feathermoss are sandy loam to silt loam at mid-slope, and silt loam to silty clay at the top. These are, respectively, Eluviated Dystric Brunisols and Orthic Eutric Brunisols (Expert Committee on Soil Survey, 1998). Soils at the bottom of the hill and in the riparian zone are silt loam to heavy clay and are classified as Orthic Gleysols or

Orthic Humic Gleysols. The forest floor is generally a mor-moder humus form for the Brunisols and a moder for the Gleysols.

Zero-tension lysimeters were installed in each plot below the forest floor (10 cm) and at a depth of 25 cm in the mineral soil (MacDonald et al., 2007). In the riparian plots, porous cup tension lysimeters (Soil Moisture Equipment, Santa Barbara, CA) were installed at depths of 10 and 25 cm in the mineral soil. Shallow groundwater was monitored with 30 cm PVC piezometers screened at depths of 1.4 and 1.8 m. The first four sets of soil solution and shallow groundwater samples (June 23 and 30, and July 6 and 14) were discarded and then re-sampled on July 30, August 31, September 21, and October 20. All isotopic analyses were performed on the samples collected on September 21, 2005, as all collectors yielded a sample.

Rainwater was collected throughout the growing season as wet-only deposition using an automated and chemically clean wet-only deposition collector (Model 200, Ecotech, Blackburn, Australia). The collector was installed on top of a 14 m high aircraft hangar that is used by the forest fire fighting crew just outside the town of La Ronge. In addition, snow cores were collected from Lac La Ronge (55° 6' 0 N; 105° 17' 60 W) and lake Nemeiben (55° 19' 60 N; 105° 19' 60 W) in March 2005, approximately 500 m from shore to avoid contamination by vegetation debris in order to obtain the best possible regional atmospheric signal. High density 20 L acid-washed polyethylene pails and lids were pre-contaminated with the snow from each lake, and snow samples were collected by driving down several times into the snow pack. The snow samples were thawed within hours of collection and ~250 ml of the melt water was transferred into pre-cleaned polyethylene bottles.

Foliage and stemwood were sampled on August 31 from one dominant or co-dominant tree, and one understory (young) tree when present, of each species in each plot. Foliage exposed to direct sunlight (located in the upper half of the canopy) was targeted and sampled using a shotgun. No attempt was made to separate foliage into age classes. Stemwood was sampled at 1.3 m from the ground using a 4.1 mm-diameter Haglöf® increment borer.

In addition to the field study, an aspen seedling was grown *in vivo* on crushed basalt (very fine sand and silt) mixed with pure quartz (fine sand) at a weight ratio of 15:1. Before planting, seed stratification was performed by soaking the seeds in a mix of water and pure quartz sand for one week. Seedlings were grown for 6 weeks in a growing chamber set at 21°C and 40% air humidity with 15 hours of sunlight per day. A Hoagland-type nutrient solution was used to feed the seedlings, except that it was Ca free. It was added every 2 to 3 days, keeping the surface soil moist to the touch. The seedling was harvested after two months of growth, and aliquots of leaf, stem, root radicle, and fine root were sampled for analysis.

### 3. ANALYTICAL METHODS

#### 3.1 Ca pools in soils and trees

Forest floor bulk density was obtained by cutting around a 20 cm × 20 cm template (slash, litter layer, moss cover, and large roots removed) and then measuring its depth and oven-dry mass. Bulk density of upper mineral soil was also assessed on oven-dried samples after sampling the soil with a bucket auger with a known volume (0-20 cm and 20-40 cm increments). The discontinuous Ae horizon of the Eluviated Dystric Brunisols (mixedwood) was not sampled because it is difficult to separate it from the forest floor and mineral soil in this setting. The product of soil bulk density and exchangeable Ca concentration was used to estimate the size of soil exchangeable Ca pools.

Allometric equations developed by Lambert et al. (2005) were employed to estimate the aboveground biomass density (organic dry mass per unit area) in each plot (Bélanger and Holmden, submitted). Stem, bark, branches, and canopy biomass were assessed individually for each species using the diameter at breast height data as input. Total aboveground Ca content in each plot was estimated as the sum of Ca content in stemwood, bark, foliage, and branches. Root biomass, not part of Lambert's equations, was estimated using above and below ground biomass

data collected on boreal species near Candle Lake, Saskatchewan (Kalyn and Van Rees, 2006). The root biomass fractions were calculated for black and white spruce, aspen, and jack pine, and applied to the La Ronge stands to estimate root biomass in each plot. The Ca content of root biomass was calculated using the Ca concentrations for branches given by Lambert et al. (2005). Branches are higher in Ca than stemwood and lower than foliage. Taking this approach, the roots added 10–20% more Ca to the vegetation pools in each study plot.

### 3.2 Sample digests and Ca concentrations

All solutions were filtered through 0.4  $\mu\text{m}$  polycarbonate membranes in a Class 10,000 trace metal clean room in the Saskatchewan Isotope Laboratory. Foliage and stemwood samples were oven-dried for 48 h at 65°C. Root samples were cleared of soil particles by repeated rinsing and sonication in ultra pure water, and checked for cleanliness using a binocular microscope. No adhering particles were observed. The dried samples were then broken up and digested in ultrapure ~15 N  $\text{HNO}_3$  using 150 to 500 ml PTFE beakers covered with PTFE ‘watch glasses’ on a hot plate at 130°C for 3 days.

One gram samples of lower B horizon mineral soil from each plot were extracted with 10 ml of 0.1 N  $\text{BaCl}_2$  solution (purity 99.999%) on a shaker for 2 hours. This served as a proxy for exchangeable cations, including Ca and Sr. The sample was rinsed and decanted several times with ultrapure water to remove excess  $\text{BaCl}_2$  and then subjected to a weak acid leach using 1 N  $\text{HNO}_3$  at room temperature for 2 hours. According to Nezat et al. (2007), this weak digest removes Ca and Sr from the crystal lattice of apatite and possibly some Ca and Sr contained in biotite and chlorite. The supernate was removed by centrifugation and the residue treated with 10 ml of 15 N  $\text{HNO}_3$  for 8 hours at 70°C. The supernate was again removed, and an aliquot of the remaining sample digested in HF- $\text{HNO}_3$ . The HF- $\text{HNO}_3$  digests remove Ca and Sr held in the more refractory minerals such as muscovite, alkali feldspar, and plagioclase (Nezat et al. 2007). A finely ground sample of the local granite was also subjected to the 1 N and 15 N  $\text{HNO}_3$  digests,

and another [sample was dissolved completely in HF-HNO<sub>3</sub>. Calcium concentrations for all samples were measured by isotope dilution thermal ionization mass spectrometry \(ID-TIMS\).](#)

### 3.3 $\delta^{44}\text{Ca}$ measurements

Aliquots of clear solutions corresponding to 50  $\mu\text{g}$  of Ca were mixed with aliquots of  $^{43}\text{Ca}$ - $^{42}\text{Ca}$  double spike to achieve a target mixed  $^{40}\text{Ca}$ / $^{42}\text{Ca}$  ratio of 7.0. The solution was then dried down, resolublized, and dried down again to promote equilibration of spike and sample isotopes. This step is performed before the samples are loaded onto the ion exchange columns. This ensures that any isotope fractionation that may occur on the columns, from yields that are less than 100%, is corrected for at the same time as the mass discrimination correction for fractionation in the mass spectrometer. The preparation and composition of the double spike is given in Holmden (2005). Calcium is purified from K and Sr using Teflon columns from Savillex® filled with 3 ml of Biorad® MP50 cation exchange resin. To minimize blank, all sample containers and pipettes were cleaned in 2 N HNO<sub>3</sub> and thoroughly rinsed in ultrapure water. Tests showed that most of the Ca blank originated from the columns and loading. The total combined column and loading blank was controlled to between 80 and 130 ng, measured by isotope dilution. The Ca blank has a ‘normal’ isotopic composition ( $\delta^{44}\text{Ca} = -1.27\text{‰}$ ) typical of the values measured in terrestrial samples. At a sample to blank ratio of 500 the blank contribution is negligible, and no correction for blank contribution was applied to the data. After the pure Ca aliquot was dried, two drops of H<sub>2</sub>O<sub>2</sub> were added and dried to help oxidize organics contributed from the column, followed by 2 drops of 15 N HNO<sub>3</sub> to convert the sample to the nitrate form for loading.

Loading was performed under a binocular microscope using a 0.5–10  $\mu\text{l}$  range digital pipette. Between 3 and 8  $\mu\text{g}$  of Ca was loaded onto single, out-gassed Ta filaments (0.00137"



thick, 0.030" wide) using parafilm dams to limit the spread of the sample. Between 0.5 and 1.0 ml of 10% ultrapure  $\text{H}_3\text{PO}_4$  was then added to the load and the solution dried, carefully, by raising the filament current. The sample does not dry completely because water is absorbed from the air as the filament current is increased. The parafilm melts, and the sample eventually boils as moisture escapes from the viscous load. The current is increased further, and boiling is allowed to continue for one or two minutes to homogenize the load, and possibly allow Ta from the filament to dissolve and mix into the load. Tantalum is known to increase Ca ionization efficiency in the mass spectrometer.

In the mass spectrometer, the filament current is increased slowly over a period of about 40 minutes until a  $^{44}\text{Ca}$  ion beam of  $\sim 50$  mV is achieved ( $10^{11}$  ohm resistor). At this point, or shortly thereafter, the ion beam intensities will increase with little or no additional increase in the filament current. Often times it will be necessary to lower the current in order to slow the rapidly increasing ion beam currents. During a run, however, the beam growth is restricted to 5%, and is checked between blocks. Initially, focusing is performed semi-automatically (i.e., with operator oversight) with the goal of maximizing the ion beam intensities and perfecting peak shape, and then by computer control once every five blocks during the run. The Ca isotope measurements are performed in three scans (or hops) of the magnetic field to restrict the mass range of the measurements to 5% in order to minimize potential ion optical effects (Fletcher et al., 1997; Holmden, 2005; and Appendix A for further details). Data collection begins when the  $^{44}\text{Ca}$  ion beam intensity is between 200 and 400 mV, with corresponding  $^{40}\text{Ca}$  intensities between 10 and 20 V. Typically, data representing 18 blocks of ten cycles each are collected. Each cycle takes 43 seconds to complete, with 30-second baselines between cycles, for a total run time of about three hours. The reason for the long analysis is to provide a sufficient record of the behavior of the run so as to confidently assess its quality, although ion-counting statistics are also improved. High quality runs show: (1) no shift in mass bias corrected ratios after focusing, (2) no drift in mass bias corrected ratios with time, and (3) a normal and steady fractionation trend with time showing

increased heavy isotope enrichment of residual Ca on the filament. Any periods of reverse fractionation, or runs characterized by erratic patterns of fractionation, signify that the Ca on the filament may be parceled into multiple reservoirs, each fractionating at different rates (e.g., Hart and Zindler, 1989; Upadhyay et al., 2008; Fantle and Bullen et al., 2009). This type of evaporation and ionization behavior on the filament greatly degrades the effectiveness of the instrumental mass bias correction and the accuracy of the data. When beam growth and isotopic fractionation are steady throughout a long run, it implies that Ca is being drawn from a single homogenous reservoir on the filament.

Three ratios are constructed from the collected data: (1)  $^{40}\text{Ca}/^{42}\text{Ca}$  from the first hop, (2)  $^{42}\text{Ca}/^{43}\text{Ca}$  from the second hop, and (3)  $^{42}\text{Ca}/^{44}\text{Ca}$  from the combined second and third hops.  $^{41}\text{K}/^{42}\text{Ca}$  is monitored in the first hop, but the ratio is so low that corrections for  $^{40}\text{K}$  interference on  $^{40}\text{Ca}$  are never required (see Appendix A for collector configuration). The mixed composition runs are corrected for instrumental mass bias, and the tracer Ca unmixed from the sample, using equations published in Eugster et al. (1969), which are solved iteratively in a spreadsheet. Calcium isotopic data are reported in the standard delta ( $\delta$ ) notation as variations in  $^{44}\text{Ca}/^{40}\text{Ca}$  relative to measurements of natural seawater. Pacific, North Atlantic, and Caribbean seawater have been measured, and it is found that their  $\delta^{44}\text{Ca}$  values are identical within the uncertainties of the measurements, in agreement with (Hippler et al. 2003). Ultimately, the reproducibility of the measurements is based on the analyst's ability to correct for instrumental drift (Appendix A) and the care and attention being paid to loading, focusing, and fractionation during the run. For these reasons we have not yet attempted to run a sequence of Ca samples under complete computer control.

The reproducibility for a single, drift-corrected measurement of  $\delta^{44}\text{Ca}$  is  $\pm 0.07\text{‰}$  ( $2\sigma$ ), which is estimated by taking the standard deviation of 90 measurements of two internal standards:  $^{41}\text{CaF}_2$  and 49 seawater, from 24 measurement sessions (each one of approximately two weeks

duration) over the last, approximately, two years. Instrumental drift is corrected for by adjusting the isotope composition of the double spike in each measurement session (using an exponential law) to achieve an average isotopic difference of  $-1.29\text{‰}$  between the two standards employed for this purpose ( $\delta^{44}\text{Ca}_{\text{CaF}_2} - \delta^{44}\text{Ca}_{\text{seawater}}$ ) (Appendix A). The drift corrected  $\delta^{44}\text{Ca}$  value of 915a measured over the past two years is  $-1.86 \pm 0.05\text{‰}$  ( $2\sigma$ ,  $n=13$ ).

#### 4. FOREST FLOOR CALCIUM MODEL

A simple model that captures the impact of forest growth on the  $\delta^{44}\text{Ca}$  values in plant available soil pools consists of two boxes (Fig. 4). The upper box is the exchangeable Ca pool of the forest floor ( $M_{FF}$ ), which represents the litter layer of the forest floor of  $\sim 10$  cm thickness. The lower box is the exchangeable Ca pool of the upper B horizon ( $M_B$ ), which represents the mineral soil of  $\sim 25$  cm thickness. The two pools are intended to cover the range of soil depths permeated by tree fine roots, which draw Ca from these pools to support forest growth. The definitions of the components and units employed are listed in Table 1.

The amount of Ca in each ion exchange pool ( $M_i$ ) is given in units of  $\text{mol m}^{-2}$ , which takes into account the thickness of the pool. Moreover, each pool is considered to be isotopically homogenous in  $\delta_i$ , and identical to the soil solutions that filtered through them into the lysimeters.

The arrows in Fig. 4 represent Ca fluxes. The principle input fluxes include soil mineral weathering ( $f_w$ ), atmospheric deposition ( $f_a$ ), and leach losses from litterfall ( $f_{lf}$ ). The principle output fluxes include plant uptake ( $f_u$ ), leach losses from the forest floor to the upper B soil mineral pool ( $f_z$ ), and leach losses from upper B to groundwater ( $f_{gw}$ ). The  $\delta^{44}\text{Ca}$  values for fluxes  $f_a$ ,  $f_w$ ,  $f_{lf}$ ,  $f_z$ , and  $f_{gw}$  are, respectively,  $\delta_a$ ,  $\delta_w$ ,  $\delta_{lf}$ ,  $\delta_{FF}$ , and  $\delta_B$ .

Equations 1.1–1.4 are the model's mass balance and isotope mass balance framework equations.

$$\frac{dM_{FF}}{dt} = f_a + f_{lf} - [f_z + f_u X] \quad (1.1)$$

$$\frac{dM_B}{dt} = f_w + f_z - [f_u (1 - X) + f_{gw}] \quad (1.2)$$

$$\frac{d(M_{FF}\delta_{FF})}{dt} = f_a \delta_a + f_{lf} \delta_{lf} - [f_u X(\delta_{FF} + \Delta_{soil}^{veg}) + f_z \delta_{FF}] \quad (1.3)$$

$$\frac{d(M_B\delta_B)}{dt} = f_z \delta_{FF} + f_w \delta_w - [f_u (1 - X)(\delta_B + \Delta_{soil}^{veg}) + f_{gw} \delta_B] \quad (1.4)$$

A close examination of the equations, and Fig. 4, shows that the atmospheric Ca flux enters the forest Ca cycle through the forest floor pool, whereas the soil mineral weathering Ca flux enters through the upper B mineral soil pool. The fraction of Ca drawn into the trees from the forest floor pool is  $X$ , and from the upper B pool  $(1 - X)$ .

Fixed parameters include the measured  $\delta^{44}\text{Ca}$  values in the soil ( $\delta_{FF}, \delta_B$ ) and vegetation pools ( $\delta_{veg}$ ), seasonally averaged precipitation ( $\delta_a$ ), soil mineral weathering ( $\delta_w$ ), and the Ca uptake flux ( $f_u$ ). The fractionation factor  $\Delta_{soil}^{veg}$  ( $=\delta_{veg} - \delta_{soil}$ ) is determined individually for each study plot (see section 5.4).

To achieve a balanced model (all Ca fluxes positive), the value of  $f_a$  is adjusted until the model derived proportions of Ca from atmospheric deposition and soil mineral weathering (mixed and immobilized in the vegetation) match the Ca apportionment constraints deduced using the  $^{87}\text{Sr}/^{86}\text{Sr}$  technique (Miller et al., 1993; Chadwick et al., 1999; Kennedy et al., 1998; Kennedy et al., 2002; Bullen and Bailey, 2005; Drouet et al., 2005; Bélanger and Holmden, submitted). A second constraint is that 80% of the trees annualized Ca requirement is from recycled litterfall, a fraction deduced by Miller et al. (1993) using the  $^{87}\text{Sr}/^{86}\text{Sr}$  tracer technique in the Adirondacks of

312 New York State (see section 5.4 for further discussion). Steady state equations, such as Eq 1.5 for  
 313  $f_w$ , are used to calculate a set of Ca fluxes for  $f_{lf}$ ,  $f_z$ ,  $f_w$ , and  $f_{gw}$ .

$$314 \quad f_w = \frac{f_a (\delta_{FF} - \delta_B) + f_{lf} (\delta_{FF} - \delta_B) + X f_u (\delta_B + \Delta_{soil}^{veg} - \delta_{FF}) - f_u \Delta_{soil}^{veg}}{(\delta_B - \delta_w)} \quad (1.5)$$

315  
 316

## 317 5. RESULTS

### 318 5.1 $\delta^{44}\text{Ca}$ in vegetation

319 Stemwood is  $^{44}\text{Ca}$ -depleted relative to soil solutions and groundwater in the same plots at  
 320 all depths (Figures 2, 3; Table 2). Foliage is  $^{44}\text{Ca}$ -enriched relative to stemwood, indicating  
 321 significant within-tree fractionation, but is  $^{44}\text{Ca}$ -depleted relative to soil and groundwater Ca  
 322 pools. Values of  $\delta^{44}\text{Ca}$  in stemwood range between  $-1.14$  and  $-1.75\text{‰}$  for five species across the  
 323 six study plots, whereas foliage values range between  $-0.64$  and  $-1.46\text{‰}$ .

324 An aspen seedling grown *in vivo* on powdered basaltic rock ( $\delta^{44}\text{Ca} = -0.88\text{‰}$ ) showed  
 325 strongly developed fractionation between the first leaves ( $-0.52\text{‰}$ ) and stem ( $-1.38\text{‰}$ ). The  
 326 seedling's roots, both radicle ( $-1.30\text{‰}$ ) and secondary ( $-1.29\text{‰}$ ), were not significantly different  
 327 from the stem. Fine root (2 mm)  $\delta^{44}\text{Ca}$  values in mature trees from the La Ronge site are lower  
 328 than stemwood values which, in turn, are lower than foliage values. A positive  $\delta^{44}\text{Ca}$  gradient  
 329 characterizes tissues formed along the transpiration stream (Wiegand et al., 2005; Holmden and  
 330 Bélanger, 2006; Perakis et al., 2006; Page et al., 2008; Cenko Tok et al., 2009).

331 Separation factors offer a convenient way to gauge the extent of Ca isotope fractionation  
 332 between different tree components and their respective soil pools (Table 3). There is a reasonably  
 333 good 1:1 correlation between  $\delta^{44}\text{Ca}$  in foliage and stemwood (Fig. 5), suggesting a robust and  
 334 stable pattern of within-tree fractionation. Some of the scatter may be due to time averaging of  
 335 possible secular trends in the  $\delta^{44}\text{Ca}$  values of stemwood, which were sampled without regard for

the age of the sampled increment. By contrast, the foliage samples reflect current growth (deciduous), or seven years of growth (conifer). The average separation factor between foliage and stemwood measured over four plots and all tree species is  $0.43 \pm 0.12\text{‰}$  (Table 3). The same average difference of  $0.41 \pm 0.05\text{‰}$  was found between stemwood and fine roots. The total average fractionation from root tips to canopy in the La Ronge forest is  $0.84\text{‰}$ , which is virtually identical to the  $0.77\text{‰}$  fractionation documented for the aspen seedling grown *in vivo*. The magnitude of within-tree fractionation of Ca isotopes between different tissues is similar among the studied tree species.

By contrast, the fractionation of Ca isotopes between the above and below ground Ca pools is about half the magnitude in jack pine compared to the other tree species. This finding is robust as it was reproduced for jack pine from three different study plots (Table 3) with differing soil pool  $\delta^{44}\text{Ca}$  values. Accordingly, the initial fractionation step in fine root tips may vary among species more widely than the internal isotope fractionation of Ca between different tree tissues. We found no consistent difference in  $\delta^{44}\text{Ca}$  values between foliage and stemwood from old (85–110 y) *vs.* young (~10–40 y) trees—the average difference (old-young) being  $-0.03 \pm 0.1\text{‰}$  ( $n=3$ ,  $1\sigma$ ).

## 5.2 $\delta^{44}\text{Ca}$ in soil pools, groundwater, and streamwater

Soil water  $\delta^{44}\text{Ca}$  values collected using lysimeters emplaced at the base of the forest floor (10 cm), selected Ah (20 cm), and upper B horizons (35 cm) are reported in Table 2 (numbers in parentheses indicate depth from surface). The soil water  $\delta^{44}\text{Ca}$  values are lower in the forest floor and higher in the mineral soils for all plots (Figs. 2, 3). To test whether the increase in  $\delta^{44}\text{Ca}$  with depth continues below the level of the fine roots (>35 cm), Ca was extracted using a  $\text{BaCl}_2$  solution from the lower B/C mineral soils at 50–65 cm depth. Although slight increases of between 0.1 and 0.2‰ are observed in three study plots (1.3, 2.1, and 2.2), the average difference

in  $\delta^{44}\text{Ca}$  value between lower B/C soil extracts and upper B soil waters from six plots is close to zero ( $0.05 \pm 0.13\text{‰}$ ,  $1\sigma$ ). This is consistent with groundwater samples collected from 1.4 and 1.8 m depths from the riparian plots (1.3 and 2.3), which yielded an average  $\delta^{44}\text{Ca}$  value of  $-0.67 \pm 0.21\text{‰}$ . This is within the uncertainty of the upper B soil waters from the same plots ( $-0.63 \pm 0.25\text{‰}$ ). These are in turn similar to eight streamwater samples collected at the base of Toposequence 1 over the course of the 2005 season, which yielded an average  $\delta^{44}\text{Ca}$  value of  $-0.61 \pm 0.05\text{‰}$  ( $1\sigma$ ).

### 5.3 $\delta^{44}\text{Ca}$ in bedrock, soil mineral weathering release, and atmospheric deposition

Wet-only deposition during the summer months was found to be lower in  $\delta^{44}\text{Ca}$  ( $-1.31\text{‰}$ ,  $n=2$ ) than winter precipitation sampled from snow pack on nearby Lac La Ronge and Nemeiben Lakes ( $-1.22\text{‰}$ ,  $n=3$ , excluding the lowest value in Table 2). From these  $\delta^{44}\text{Ca}$  data a weighted average value of  $-1.28\text{‰}$  is calculated for a mixture of 30% snowmelt and 70% summer precipitation.

A whole-rock HF- $\text{HNO}_3$  digest of the granite bedrock yielded a  $\delta^{44}\text{Ca}$  value of  $-1.27\text{‰}$ , which is virtually identical to the annualized  $\delta^{44}\text{Ca}$  value in precipitation. Because Ca release from granite weathering is non-stoichiometric owing to differences in mineral solubilities, the granite was powdered and leached sequentially with 1 N and 15 N  $\text{HNO}_3$  solutions. The 15 N acid leachate ( $-1.57\text{‰}$ ) was lower in  $\delta^{44}\text{Ca}$  than the totally digested whole-rock ( $-1.27\text{‰}$ ) and the 1 N  $\text{HNO}_3$  leachate ( $-1.36\text{‰}$ ) (Table 2). This finding is consistent with the hypothesis of preferential release of radiogenic  $^{40}\text{Ca}$  from biotite dissolution, which is supported by the pattern of  $^{87}\text{Sr}$  release (Bélanger and Holmden, submitted) (Table 2).

To obtain a more realistic estimate of the  $\delta^{44}\text{Ca}$  signature of soil mineral weathering, samples from the lower B/C horizons in each study plot were subjected to weak and concentrated  $\text{HNO}_3$  acid leaches after first removing the exchangeable Ca ions using a 0.1 N  $\text{BaCl}_2$  solution.

The results are listed in Table 2 and plotted in Fig. 6 against their corresponding  $^{87}\text{Sr}/^{86}\text{Sr}$  ratios. Although the sequential treatment yielded increasingly radiogenic  $^{87}\text{Sr}/^{86}\text{Sr}$  ratios in the leachates, the less negative  $\delta^{44}\text{Ca}$  values indicate that a large fractionation of the co-released Ca bears the heavy isotope signature of plant-induced fractionation. This means that a sizeable fraction of the Ca and Sr in the leachates does not come from the weathering of pristine igneous minerals, but rather, has filtered down from the upper B horizon and become trapped in secondary mineral growth (e.g. interlayers of clays), and/or captured by (less exchangeable) ion exchange sites. Taking a closer look at the trends in Fig. 6 reveals two ‘plateau values’ that further leaching will unlikely change. The coarser textured soils of plots 1.1 and 1.2 reached  $-1.06 \pm 0.01\text{‰}$ . The other four plots reached  $-1.16 \pm 0.02\text{‰}$ . This finding is consistent with the relatively small range of  $\delta^{44}\text{Ca}$  values among igneous minerals compared to the relatively large range in  $^{87}\text{Sr}/^{86}\text{Sr}$ . As a case in point, during the leaching of the granite powder,  $\delta^{44}\text{Ca}$  values decreased by just 0.3‰, which reflects preferential dissolution of  $^{40}\text{Ca}$  enriched biotite. By contrast, the corresponding change in  $^{87}\text{Sr}/^{86}\text{Sr}$  is 260‰ owing to the high levels of  $^{87}\text{Rb}$  in biotite and the  $\sim 1.85$  Ga age of the granite.

#### 5.4 Plot specific vegetation–soil fractionation factors

The Ca isotope fractionation factor ( $\Delta_{\text{soil}}^{\text{veg}}$ ) is an important quantity that requires careful consideration. The separation factors listed in Table 3 were calculated without taking into account the isotope mass balance of Ca between different tree tissues. Calcium translocation in trees causes isotopic fractionation of Ca, as evidenced from the differences in  $\delta^{44}\text{Ca}$  values between foliage and stemwood (Table 2). Yet, there must be a primary fractionation step that occurs in the root tips of the fine roots because the  $\delta^{44}\text{Ca}$  values of the soil pools are  $^{44}\text{Ca}$  enriched ( $-0.45$  to  $-1.05\text{‰}$ ) relative to Ca inputs from atmospheric deposition ( $-1.28\text{‰}$ ), soil mineral weathering ( $-1.06$  to  $-1.16\text{‰}$ ), and foliage ( $-1.15$  to  $-1.36\text{‰}$ ) the principal component of litterfall (Table 4).



The first step towards calculating a bulk fractionation factor for the stands in each plot is to compute the  $\delta^{44}\text{Ca}$  values of each tree species from the Ca mass fractions and  $\delta^{44}\text{Ca}$  values of the major tree tissues using the Ca allometry (Table 4), and then computing  $\delta_{veg}$  by weighting whole-tree  $\delta^{44}\text{Ca}$  values for each species against the species biomass distribution in the plot (Table 4).

The soil pools present a different problem. A  $\delta^{44}\text{Ca}$  value is needed that reflects the impact of the Ca taken up by plants, so that the fractionation factor can be calculated by difference ( $\delta_{veg} - \delta_{soil}$ ). But trees draw Ca from pools in the forest floor and mineral soil, which differ in their  $\delta^{44}\text{Ca}$  values. Therefore, we cannot determine  $\Delta_{soil}^{veg}$  without first considering how the uptake of Ca into the trees is split between Ca pools in the forest floor ( $X$ ) and upper B mineral soil ( $1 - X$ ). This is done through the use of a simple mixing equation (Eq. 1.6) that relates changes in  $\Delta_{soil}^{veg}$  to  $X$  using measured values of  $\delta_{veg}$ ,  $\delta_{FF}$ , and  $\delta_B$ :

$$\Delta_{soil}^{veg} = (\delta_{veg} - \delta_B) - X(\delta_{FF} - \delta_B) \quad (1.6)$$

At the present time, we cannot determine  $\Delta_{soil}^{veg}$  independently from  $X$ , thus, we employ the steady state equations and trial values of  $\Delta_{soil}^{veg}$  to calculate a trial set of model Ca fluxes for each plot. These fluxes, in turn, are used to calculate two additional quantities: (1) the fraction of Ca in vegetation that is derived from atmospheric deposition vs. soil mineral weathering, which must match the Ca apportionment constraints deduced from the  $^{87}\text{Sr}/^{86}\text{Sr}$  study (Bélanger and Holmden, submitted), and (2) the fraction of the forest's annualized Ca requirement that is internally cycled through litterfall, which we set at 80% of the total Ca inputs to the forest. The value for  $\Delta_{soil}^{veg}$  is adjusted until conditions (1) and (2) are satisfied. Taking this approach, the average value of  $X$  is  $0.64 \pm 0.12$  ( $1\sigma$ ), and the average value of  $\Delta_{soil}^{veg}$  is  $-0.70 \pm 0.13$  ( $1\sigma$ ) (Table 5). How closely the model results approach the magnitudes of the true Ca fluxes depends on four sources of uncertainty: (1) the degree to which the measured  $\delta$ -values genuinely reflect the Ca

pools to which they are assigned, (2) the validity of the  $^{87}\text{Sr}/^{86}\text{Sr}$  based study of Ca partitioning between atmospheric and soil mineral weathering sources in trees, (3) the appropriateness of the assumption that 80% of the annualized Ca input to the forest Ca cycle is from litterfall, and (4) the accuracy of the plant uptake Ca flux ( $f_u$ ).

## 5.5 Model results

### 5.5.1 Steady state solutions

Forest growth rates are typically highest during the middle stage of development, which corresponds to important increments in stemwood volume (Miller, 1995). Since the La Ronge forest is mature, most of the trees' resources are presently directed towards maintaining the canopy; thus, its current growth rate is relatively low. Accordingly, the Ca uptake rate in the mature forest is broadly equivalent to the amount of Ca needed to support the annual turnover of foliage in the canopy, which may be deduced from the Ca allometry. It follows that we calculated the mass of Ca in the deciduous leaves (dividing by the average hang time of one year) and conifer needles (dividing by the average hang time of seven years) in each plot, and then summed the results to determine the annualized Ca uptake for each plot. Values of  $f_u$  scale positively with the values of  $f_a$ ,  $f_w$  and  $f_{lf}$ , as dictated by the isotope mass balance constraints imposed by the measured  $\delta^{44}\text{Ca}$  values in each soil pool. Consequently, if  $f_u$  is underestimated,  $f_a$ ,  $f_w$  and  $f_{lf}$  will also be underestimated. The correct evaluation of the Ca uptake flux will, in principle, lead to accurate evaluations of several other Ca fluxes that are otherwise difficult to determine, such as the soil mineral weathering flux ( $f_w$ ; Eq. 1.5), or leach losses of Ca to groundwater ( $f_{gw}$ ). The model values for these fluxes are computed individually for each study plot and listed in Table 5.

The average Ca weathering flux predicted by the Ca cycling model ( $0.019 \text{ mol m}^{-2} \text{ y}^{-1}$ ; Table 5) is in good agreement with PROFILE—a steady state model developed to reconstruct

release rates of base cations from soil mineral weathering—yielding  $0.025 \text{ mol m}^{-2} \text{ y}^{-1}$ . PROFILE modeling is based on kinetic rate laws (Sverdrup, 1990) and the chemical composition of the forest soil (Sverdrup and Warfvinge, 1995). The above result was obtained by modeling the first 50 cm of soil for each plot. Input variables included empirical mineralogy (Bélanger and Holmden, submitted), specific surface area, soil water content, and soil temperature. Specific surface area of the soil was calculated from an algorithm developed by Jönsson et al. (1995) using measured grain size distribution, dry bulk density, and coarse fragments. Soil temperature was estimated using the FORSTEM model (Yin and Arp, 1993).

The average Ca deposition flux predicted by the Ca cycling model ( $0.015 \text{ mol m}^{-2} \text{ y}^{-1}$ ; Table 5 and Fig. 7) is within the range of wet only deposition fluxes for the Province of Saskatchewan of between  $0.002$  and  $0.030 \text{ mol m}^{-2} \text{ y}^{-1}$  (Canadian National Atmospheric Chemistry Precipitation Database, 1978-1992). On the other hand, if seasonally averaged Ca concentrations in precipitation from La Ronge are used from Table 2 ( $\sim 0.32 \text{ ppm}$ ), then the annualized atmospheric deposition flux is  $0.0024 \text{ mol Ca m}^{-2} \text{ y}^{-1}$ , which is closer to the low end of the provincial range represented by Cree Lake (average of  $0.002 \pm 0.002 \text{ mol Ca m}^{-2} \text{ y}^{-1}$  measured between 1978 to 1992), one of the most pristine sites monitored in northern Saskatchewan. It is important to note that the model estimation from Ca cycling is for wet and dry deposition combined, whereas the provincial estimates are wet only deposition. Dry deposition would need to be  $\sim 4$  times higher than wet deposition to make up the difference.

### 5.5.2 Transient solutions

The impact of changing one or more Ca fluxes on soil pool  $\delta^{44}\text{Ca}$  values was investigated using the transient equations (1.3, 1.4) and the initial steady state Ca fluxes of plot 1.1 (Table 5). Although a number of model runs were performed, two are highlighted below. The first one documents changes in soil and vegetation pool  $\delta^{44}\text{Ca}$  values caused by a step increase in Ca

uptake rate, which informs on the effects of differences in forest productivity in different regions. The second one was undertaken to show the effect of changing the proposed species-specific fractionation factor.

The impact of increasing the plant uptake flux ( $f_u$ ) by 50% over the steady state value is shown in Fig. 8. This causes Ca concentrations to decrease in the forest floor and upper B mineral soils, as expected, and  $\delta^{44}\text{Ca}$  values to increase. Vegetation  $\delta^{44}\text{Ca}$  increases too, because the trees respond by tracking the changes in  $\delta^{44}\text{Ca}$  in the soil pools. The extent to which the soil pools record a heavy Ca isotope signature depends on the magnitude of the Ca uptake flux ( $f_u$ ) relative to the Ca input fluxes ( $f_a$ ,  $f_{lf}$ , and  $f_w$ ). This is shown by imposing a co-occurring increase of three times the steady state flux of  $f_a$ , which is enough to reverse the increase in soil pool  $\delta^{44}\text{Ca}$  caused by a 50% increase in  $f_u$  (not shown). The second model run demonstrates the impact of increasing  $\Delta_{soil}^{veg}$  by 2.8 times and  $f_u$  by 1.4 times, which causes  $\delta^{44}\text{Ca}$  values between soil and vegetation pools to widen from an initial steady state separation factor of  $-0.7\text{‰}$  ( $\delta_{veg} - \delta_B$ ) to a final separation factor of  $-2.3\text{‰}$  (Fig. 9). These changes to the La Ronge forest Ca cycle reproduces the difference in  $\delta^{44}\text{Ca}$  values reported by Schmitt et al. (2003) between a beech branch and soil pool measured in a forest in France.

Other simulations were conducted, but the results are not shown. One of these examined the impact of changing the Ca uptake fractions between the forest floor and upper B mineral soil on soil pool  $\delta^{44}\text{Ca}$  values. Smaller soil depth gradients in  $\delta^{44}\text{Ca}$  were produced in model runs when most of the Ca was drawn from the forest floor ( $X \approx 1$ ). Larger depth gradients were produced when most of the Ca was drawn from the upper B horizon ( $X \approx 0$ ). The magnitude of the output flux,  $f_u$ , relative to the input fluxes  $f_a$ ,  $f_{lf}$ ,  $f_z$ , and  $f_w$  is another factor that influences the magnitudes of the soil depth gradients. For example, if the downward flux of Ca ( $f_z$ ) from the forest floor is much higher than the plant uptake flux from the upper B horizon,

then the upper B Ca pool will mostly inherit the  $\delta^{44}\text{Ca}$  value of the forest floor Ca pool, and the depth gradient will be greatly diminished. Another model run (not shown) predicts that reverse gradients will occur in cases where soil mineral weathering rates are high, and fine root activity is concentrated in the forest floor. No reverse gradients were found among the six Boreal Shield soil profiles studied in this work.

## 6. DISCUSSION

### 6.1 Tracer potential of $\delta^{44}\text{Ca}$ in forested watersheds

The results confirm previous findings that nutrient Ca uptake by plants is a significant source of isotopically fractionated Ca on the continents (Schmitt et al., 2003; Bullen et al., 2004; Wiegand et al., 2005; Holmden and Bélanger, 2005; Perakis et al., 2006; Page et al., 2008; Cenkci Tok et al., 2009). The separation factors indicate that plant uptake favors the light isotopes of Ca, which leaves the soil pools enriched in the heavy isotopes. Calcium inputs from soil mineral weathering ( $-1.06$  to  $-1.16\text{‰}$ ) and atmospheric sources ( $-1.28\text{‰}$ ) yield similarly low  $\delta^{44}\text{Ca}$  values and, therefore, cannot account for the heavy  $\delta^{44}\text{Ca}$  signatures in the soil pools, groundwater, or the stream. The total range of fractionation in the Boreal Shield forest, the largest terrestrial biome on the planet, is  $\sim 1.6\text{‰}$ . Values as high as  $-0.45\text{‰}$  characterize deeper soils and shallow groundwater, and values as low as  $-2.2\text{‰}$  characterize tree fine roots. Considering that fine roots (2.0 mm) are a small component of the total mass of Ca in boreal tree species, a smaller range of  $\sim 1\text{‰}$  is of greater relevance in this region.

Once plant fractionated Ca percolates below the finely rooted zone, it is no longer subjected to biological fractionation effects, and only mixing with other sources of Ca may further alter its signature. This makes  $\delta^{44}\text{Ca}$  a fairly unique hydrological tracer in forested catchments because the heavy isotopic signature traces the source of Ca to the forest floor and upper mineral soil (Schmitt et al., 2003; Holmden and Bélanger, 2006; Cenkci Tok et al., 2009).

There are two possible exceptions to this rule. One concerns arid environments (Ewing et al, 2008) where soil water conditions are suitable for calcite and gypsum precipitation. The light isotopes of Ca are partitioned favorably into these minerals, leaving the residual Ca in soil pore fluids enriched in the heavy isotopes. The kinetic isotope fractionation governing calcite and gypsum precipitation mimics the isotopic effects associated with plant uptake fractionation, and it may be difficult in some environments to distinguish between them (e.g., Tipper et al., 2006; Jacobson and Holmden, 2008). In acidic soils such as those of the Boreal Shield forests near La Ronge, these Ca-bearing minerals do not form. It is therefore an unlikely mechanism for producing heavy isotope enrichments in groundwater and surface water in Boreal Shield environments.

The other exception concerns potential isotopic fractionation effects associated with ion exchange reactions (Russell and Papanastassiou, 1978b). Because Ca filters downward through the soil, its  $\delta^{44}\text{Ca}$  value may be increased if  $^{40}\text{Ca}$  is preferentially retained on ion exchange sites. A lack of data on ion exchange effects prompted us to ignore the interaction between soil pore waters and ion exchange pools in our model. It is assumed, for example, that the  $\delta^{44}\text{Ca}$  values of soil waters collected by the lysimeters genuinely reflect the  $\delta^{44}\text{Ca}$  values of the Ca exchange pools, and that isotope fractionation effects accompanying ion exchange reactions are small. We also do not attach much importance to the modeled Ca residence times for the pools of the forest floor and upper B horizons because their Ca masses are operationally defined. Nevertheless, the 85-year-old stands in plots 1.1, 1.2 and 2.2, which yielded relatively small Ca soil pools by the  $\text{BaCl}_2$  technique, have apparently attained steady state, but that the remaining plots will not reach steady state in this current rotation of the forest. Recalling that the  $\delta^{44}\text{Ca}$  values of the soil pools are based on soil waters collected using lysimeters, it seems likely that as long as the Ca in these soil waters genuinely reflects the balance of the competing input and output Ca fluxes, then the most mobile fraction of the total Ca exchange pool will be close to steady state in all of the plots.

Although some details must await further study, the potential for  $\delta^{44}\text{Ca}$  as a hydrological tracer in forested catchments seems promising (Schmitt et al. 2003; Cenki Tok et al., 2009). A mixing calculation shows that more than 80% of the Ca in the stream carries the heavy isotopic fingerprint of the exchange pools from the surrounding forest soils. This finding is consistent with conceptual models of shallow groundwater flow in first-order watersheds of the Precambrian Shield. During the growing season, these watersheds are largely fed by shallow groundwater near the stream and in direct contact with bedrock (Hill 2000). When it rains, the water table in the saturated (riparian) zone rises and connects subsurface flow from the hillslope to the stream. The lower B and C horizons are common end-members contributing to the stream during high flows (Buttle and Sami 1992; O'Brien and Hendershot 1993), whereas contributions from the forest floor and uppermost mineral soil occur only during floods and large snowmelt events (Bishop et al. 1990; Hruska et al. 2001). For example, the hydrograph separation in O'Brien and Hendershot (1993) showed that the lower mineral soil (solum) close to the stream was responsible for as much as 80% of stream discharge in the summer and fall during large rain events. Moreover, overland flow is normally absent in the presence of moss and well developed forest floors, and direct contributions of rainfall to the stream are small due to its very small surface area. In the spring, snowmelt can be a large and rapid contributor to stream discharge, but this hydrological end-member is generally short-lived (Hill 2000).

In the studied watershed, all indications are that the hydrology is similar the above conceptual model. The effect of spring snowmelt on stream discharge is no longer observable by mid-May, two weeks following complete snow melt. The stream responded slightly to large rain events that occurred between mid-May and mid-June, perhaps due to snow-melt saturated riparian soils or remaining patches of frozen soils, both favoring rapid subsurface flow to the stream. Between mid-June and September, however, changes in stream discharges during rainfall were barely observable, indicating the dominance of steady groundwater feedings. Overland flow was never observed, even when we were sampling during intense rain events. The relatively

uniform and high  $\delta^{44}\text{Ca}$  value of streamwater in the La Ronge watershed, measured at the base of Toposequence 1 ( $-0.61 \pm 0.05\text{‰}$ ,  $1\sigma$ ) eight times in four months during the growing season, confirms that direct Ca inputs to the stream from precipitation and surface runoff are minor in this setting.

## 6.2 Implications for weathering and Ca apportionment studies in trees using $^{87}\text{Sr}/^{86}\text{Sr}$

A growing body of work using Sr isotopes has shown that a large fraction of the Ca that is tightly cycled between vegetation and the forest floor is ultimately derived from atmospheric sources (Miller et al., 1993; Stewart et al., 1998; Chadwick et al., 1999; Kennedy et al., 1998; 2002; Bullen and Bailey, 2005; Drouet et al., 2005). Recent work at La Ronge shows that Boreal Shield forests are no exception to this phenomenon (Bélanger and Holmden, submitted). Simple end-member mixing analysis using  $^{87}\text{Sr}/^{86}\text{Sr}$  and Sr/Ca ratios applied to the six study plots from both toposequences revealed that the amount of atmospherically-derived Ca in aspen, spruce, and jack pine varied with landscape position. Hilltop stands sequestered more Ca from atmospheric sources (85–94%) than stands at middle (47–62%) and low (37–56%) elevations (Table 5).

The estimates for atmospheric Ca contributions were strongly tied to the results of 1 N  $\text{HNO}_3$  leaches performed on lower B mineral soils in each plot, for the purpose of deducing soil mineral weathering  $^{87}\text{Sr}/^{86}\text{Sr}$  signatures (Bélanger and Holmden, submitted). However, simulating natural weathering of polymineralic soils in the laboratory with acid solutions is not straightforward (Blum et al., 2002, Bullen and Bailey, 2005, Drouet et al., 2005). Differences in  $^{87}\text{Sr}/^{86}\text{Sr}$  ratios exist among minerals, and differences in mineral weathering susceptibility yield non-stoichiometric patterns of Sr release (e.g., Blum and Erel, 1997; Nezat et al., 2007). Moreover, if the acid treatments are applied to lower B/C mineral soils there is the additional problem of overprinting by isotopes of Sr that have filtered down from overlying soil horizons.



This downward flux of Sr is dominated by litterfall whose  $^{87}\text{Sr}/^{86}\text{Sr}$  ratios reflect mixing between atmospheric deposition and soil mineral weathering sources. Caught up on ion exchange sites, or incorporated into weathered minerals, this recycled Sr must be removed before the pristine soil mineral weathering  $^{87}\text{Sr}/^{86}\text{Sr}$  signature can be revealed. The problem is that the  $^{87}\text{Sr}/^{86}\text{Sr}$  ratio of the recycled Sr component is difficult to distinguish from mineral weathering Sr component in acid leached polymineralic soils. Fortunately, this is less of a problem for Ca isotopes, due to the unique heavy isotope signature of plant-fractionated Ca. Calcium isotopes may be used to monitor the release of recycled Sr from mineral soils, thus, fine tuning the leach protocol. An examination of Fig. 6 shows that the 1 N  $\text{HNO}_3$  leach failed to remove the heavy  $\delta^{44}\text{Ca}$  signature of Ca in all but two of the study plots. This means that the  $^{87}\text{Sr}/^{86}\text{Sr}$  signature of soil mineral weathering was likely underestimated in Bélanger and Holmden (submitted) for plots 1.2, 1.3, 2.1, and 2.3 and the long-term dependence of the boreal forest on atmospheric Ca contributions will be slightly greater than originally calculated (Table 5).

### 6.3 Model validation and implications for future work

If the atmospherically derived model Ca fluxes are correct, then the dry deposition Ca flux in the La Ronge area would have to be ~4 times higher than the wet deposition flux, which seems elevated. Judging from the very high 75<sup>th</sup> and 90<sup>th</sup> percentile Ca concentrations in wet deposition computed from the Cree Lake database, there are rain events we did not capture in our limited sampling that may be bringing in significant amounts of Ca from drier agricultural regions located south of the city of Prince Albert (Fig. 1), which can carry significant amounts of Ca as particulates. Indeed, a study of the impacts of a base metal smelter located at the southern edge of the Precambrian Shield on the Saskatchewan-Manitoba border, East of La Ronge (McMartin et al., 1999) showed that the winds are mostly coming from the northwest but also noted a frequency of about 30% of winds coming from the south, southwest, or southeast. Taking this

into consideration lowers the divergence between modeled (wet plus dry) and measured (wet only) Ca fluxes.

Alternatively, one or more of the model assumptions may be contributing to the relatively high atmospheric Ca fluxes. A sensitivity analysis reveals two sources of uncertainty that warrant further investigation. The first is the uptake flux ( $f_u$ ), which scales positively with the atmospheric deposition flux ( $f_a$ ). If  $f_u$  is overestimated, then  $f_a$  will be overestimated, as well, but the uncertainty in  $f_u$  is probably less than 20%, which is too small to significantly change the large total atmospheric deposition flux calculated by the model. The second source of uncertainty involves the  $\delta^{44}\text{Ca}$  value of litterfall ( $\delta_{lf}$ ), which was assumed to be equivalent to the  $\delta^{44}\text{Ca}$  value of foliage in each plot. Indeed, a sensitivity analysis aimed at reducing the overall atmospheric deposition flux reveals that small adjustments can be made to the value of  $\delta_{lf}$  in each study plot ( $\pm 15\%$ ) that will result in an overall reduction of  $\sim 50\%$  in the value of  $f_a$ . The Ca deposition flux averaged overall all six study plots drops from  $0.015$  to  $\sim 0.008 \text{ mol m}^{-2} \text{ y}^{-1}$ . Because the modeled Ca fluxes remain tuned to the Ca apportionment fractions deduced from the  $^{87}\text{Sr}/^{86}\text{Sr}$  study (Table 5; Bélanger and Holmden, submitted), the weathering flux decreases, as well, and the proportion of recycled Ca from litterfall increases from 80 to 90% of the annualized Ca inputs to the forest Ca cycle. The high Ca recycling rate is consistent with Dijkstra and Smits (2002), who showed that only small amounts of Ca uptake from deep soils beneath sugar maple trees were needed to sustain the relatively high amounts of available Ca in the surface soil, due to tight cycling of Ca through litterfall. Similar results were presented by Miller et al. (1993), upon which we based our original estimate of  $\sim 80\%$  recycling. Accordingly, our model of low Ca release from soil mineral weathering, low Ca deposition rates, and tight Ca recycling, seems reasonable in the light of these other studies.

We conclude that the application of the Ca cycling model to the La Ronge forest is too assumption bound to yield accurate estimates of the Ca fluxes. The main problem stems from the fact that the principal input Ca fluxes are not that widely separated from in this boreal shield setting (Table 2 and Table 4), which means that relatively small percentage changes in the input  $\delta^{44}\text{Ca}$  values leads to rather large changes in the estimations of the modeled Ca fluxes. This raises the question of site selection for future studies. The  $\delta^{44}\text{Ca}$  value of precipitation and soil mineral weathering should be widely separated from each other, and the litterfall return fluxes, to yield more robust estimates of Ca flux magnitudes using isotope balance modeling. Thus far, precipitation  $\delta^{44}\text{Ca}$  values ranging between  $-0.7$  and  $-1.7\text{‰}$  have been reported (Schmitt and Stille, 2005; Cenki Tok et al., 2009), but precipitation values close to zero per mil may exist in coastal regions where Ca in rainwater is dominated by sea spray. Because most bedrock carbonates and silicates have  $\delta^{44}\text{Ca}$  values of around  $-1\text{‰}$  (DePaolo, 2004; Amini et al., 2008), field sites where precipitation values are at the extremes of the natural range may be best suited for modeling studies. A forest containing trees with a large species fractionation factor (such as beech) will help to distinguish litterfall from soil mineral weathering. In addition, a better grasp of the factors controlling litterfall  $\delta^{44}\text{Ca}$  values will be important, because the litterfall flux is the largest annualized input of Ca to the forest Ca cycle.

## 7. CONCLUSIONS

Calcium isotope fractionation occurs in tissues formed along the transpiration stream in five boreal tree species. Fine roots yielded the lowest  $\delta^{44}\text{Ca}$  values, stemwood values were intermediate, and foliage values were the highest, consistent with earlier findings (Schmitt et al., 2003; Wiegand et al., 2005; Holmden and Bélanger, 2006; Page et al., 2008; Cenki Tok et al., 2009). Plant uptake favors the light isotopes of Ca, thus leaving the residual Ca in soil pools enriched in the heavy isotopes. This implies an initial fractionation step in the tips of the fine

roots ( $\Delta_{soil}^{veg}$ ) whose magnitude appears to vary between species, but may also be subject to local environmental controls (e.g., Page et al., 2008). Data on trees from this study and from the literature (Schmitt et al., 2003; Bullen et al., 2004; Wiegand et al., 2005; Perakis et al., 2006; Page et al., 2008; Cenki Tok et al., 2009) suggest that the degree of plant induced fractionation increases in the sequence: jack pine < black spruce  $\approx$  trembling aspen  $\approx$  white spruce  $\approx$  ohia < beech  $\approx$  sugar maple.

Experiments performed using a steady state Ca cycling model showed that the degree of heavy isotope enrichment of Ca in soils is dependent on the calcium uptake rate into trees, the magnitude of the fractionation factor, and the supply rates of  $^{40}\text{Ca}$  enriched input fluxes from litterfall, atmospheric deposition, and soil mineral weathering. If these latter fluxes are high compared to the plant uptake flux, then the degree of  $^{44}\text{Ca}$  enrichment in plant available soil pools is diminished. All six study plots at La Ronge, however, show clear increases in soil water  $\delta^{44}\text{Ca}$  values with depth, ranging between 0.1 and 0.4‰. The  $\delta^{44}\text{Ca}$  depth gradient appears to be the most strongly developed where fine roots permeate the forest floor and upper B horizons, leveling off in the deeper levels of the soil where no fine roots are found. This is evidence that soil depth profiles (Perakis et al. 2008; Page et al. 2008; Cenki-Tok et al. 2009) are mostly caused by the extraction of light Ca by tree fine roots rather than by ion exchange effects involving soil mineral surfaces and organic ligands. It also implies that below the level of fine root activity, stable Ca isotopes will behave as conservative tracers of Ca transport in soil waters, groundwaters, and surface waters, so long as the ion exchange fractionation effects are small.

Calcium isotopes offer a new perspective on weathering and Ca apportionment studies of tree nutrition using  $^{87}\text{Sr}/^{86}\text{Sr}$  as a tracer. It is particularly challenging to apply the  $^{87}\text{Sr}/^{86}\text{Sr}$  technique to forests growing on acidic soils developed from granitic parent materials, due to the large differences in mineral solubility and  $^{87}\text{Sr}/^{86}\text{Sr}$  ratios. In addition, soils are contaminated with recycled Sr released from degrading litterfall with  $^{87}\text{Sr}/^{86}\text{Sr}$  ratios that reflect mixing of

isotopically distinct atmospheric and soil mineral weathering end-members. The unique heavy isotope signature of plant fractionated Ca in natural soils offers a new tool for studying Ca release from minerals and ion exchange sites in the laboratory by various treatments.

The finding that Ca isotopes are fractionated between trees and soils (Schmitt et al. 2003; Wiegand et al. 2005; Holmden and Bélanger, 2006; Perakis et al. 2008; Page et al. 2008; Cenk-Tok et al. 2009) brings the power of steady state and transient isotope mass balance modeling to bear on a variety of questions concerning Ca cycling in forests. The soil depth gradient in  $\delta^{44}\text{Ca}$  is reproduced by the model, as is the range of isotopic fractionation in forested ecosystems reported in the literature, thus far, by adjusting forest productivity (Ca uptake rate) and bulk fractionation factor. We have shown that the Ca cycling model yields reasonable sets of relative Ca fluxes for the La Ronge forest using the steady state assumption. Accuracy is compromised, however, by the small range of  $\delta^{44}\text{Ca}$  values found among the principle input Ca fluxes in the boreal shield ecosystem. Transient solutions to the isotope mass balance equations suggest that tree ring cellulose may record secular variations in  $\delta^{44}\text{Ca}$  caused by natural and anthropogenic disturbances to the forest Ca cycle.

## ACKNOWLEDGMENTS

Tim Prokopiuk is thanked for assistance in the laboratory. We also thank A. Taylor, S. Friessen, M. Emigh, J. Jackson and N. Roberston for their hard work in the field and laboratory. Dimiti Papanastassiou is thanked for advice and assistance concerning the mass spectrometry of calcium, and for hosting C.H. during a sabbatical visit to Caltech in 2003. C.H. also thanks Johannes Schwieters for communications that have guided certain tests, and clarified some of the findings reported in Appendix A. The field study and sampling was made possible *via* the financial support to N. Bélanger from the Natural Science and Engineering Council of Canada (Discovery grant). The authors thank Frank Podosek (editor) and associate editors Alan Brandon

and Martin Novak for their comments and handling of the review process. We thank two anonymous reviewers whose careful reading of the manuscript helped to improve the presentation.

## APPENDIX A. FACTORS INFLUENCING HIGH PRECISION MEASUREMENTS OF Ca ISOTOPES

It is widely acknowledged that Ca isotopes are difficult to measure (e.g., DePaolo, 2004), but for reasons that are not entirely clear. Over the past ten years, the range of precision reported in the literature has varied widely. DePaolo et al. (2004) reported good internal precision ( $\sim 0.05\text{‰}$ ) for Ca isotope measurements using a multi-collector technique on a VG 354 instrument, but poor sample reproducibility (external precision,  $\pm 0.5\text{‰}$   $2\sigma$ ). This was attributed to subtle ion beam focusing differences between samples. Fletcher et al. (1997) also reported difficulties with static multi-collection measurements on a VG 354 instrument and believed that ion optical effects were to blame. Heuser et al. (2002) published a multi-collection routine for Ca isotope measurements on a Finnigan-MAT 262 instrument, but were unable to show improved external precision over single collector peak hopping measurements performed on the same instrument ( $\pm 0.25\text{‰}$ ,  $1\sigma$ ). Because  $^{44}\text{Ca}/^{40}\text{Ca}$  variability in the sub  $\sim 1\text{‰}$  range is common, any improvement in precision and accuracy that may be related to mass spectrometer performance, choice of double spike, sample loading, or the limitations of the instrumental mass fractionation law, would be a welcome advance. For this reason, we briefly describe our experience measuring Ca isotopes in the Saskatchewan Isotope Laboratory (SIL) over the past four years, including the adopted best practices for achieving reproducibility of  $\pm 0.07\text{‰}$  ( $2\sigma$ ) on the  $^{44}\text{Ca}/^{40}\text{Ca}$  ratio.

The Ca isotope measurements were performed on a Thermo-Finnigan Triton instrument using a  $^{43}\text{Ca}$ - $^{42}\text{Ca}$  double spike to correct for instrumental mass fractionation. The rationale for using  $^{43}\text{Ca}$ - $^{42}\text{Ca}$ , as opposed to more common double-spikes with  $^{48}\text{Ca}$ , is discussed in Holmden

(2005) and Gopalan et al. (2006). The initial motivation was to restrict the mass range of the four isotopes needed for a mass bias corrected measurement of  $^{44}\text{Ca}/^{40}\text{Ca}$  to 5% by making the measurements in two scans or ‘hops’ of the magnetic field. Since then, a third hop was added so that all isotope ratios could be constructed from ion beams that were collected symmetrically with respect to the ion optical axis of the instrument. It was reasoned that this configuration would allow ion beams to strike their respective collectors in roughly the same place, at roughly similar angles to the image plane of the detector array, thus coming as closely as possible to negating potential differences in cup efficiencies that might result from non-linear changes in ion optical properties across the collector array (Fletcher et al., 1997). The collector configuration used is shown in Fig. 10.

Moreover, performing the measurements in a sequence of hops enables the signal integration times to be optimized for differences in ion beam intensities of the collected masses (particularly severe for the Ca mass spectrum, which consists of one abundant isotope and five minor isotopes). This flexibility allows scans of the smaller ion beams to be integrated for longer periods of time, thus improving the ion counting statistics, while at the same time limiting the collection of the largest ion beam ( $^{40}\text{Ca}$ ) to a short integration time in order to limit any potential degradation in the performance of the collector (Fig 10). In addition, potential  $^{40}\text{K}$  interference on  $^{40}\text{Ca}$  can be monitored using the  $^{41}\text{K}$  abundance measured in the axial collector of the first scan.

With ion optical effects minimized a suspected drift in instrument performance could be better evaluated. It had been noticed over the course of development that there were significant periods of a few weeks duration when the reproducibility of Ca isotope standards was significantly better than at other times. We attributed this drift to changes in collector efficiencies. In an attempt to solve this problem we first installed new graphite collectors in October 2006. After changing the graphite collectors, the first measurements of the  $\text{CaF}_2$  and Pacific seawater standards came out 0.19‰ lower in  $\delta^{44}\text{Ca}$  value, which seemed to confirm cup damage, but the standards changed again within a few weeks of installing the new cups (Fig. 11).

Figure 11 was constructed using data from 43 measurement sessions conducted over the past, approximately, three years. Each session included measurements of the SIL CaF<sub>2</sub> ‘isotopic normal’ as well as natural seawater. Some sessions also included measurements of SRM 915a. To account for the instrumental drift, the spike composition was adjusted for each session using an exponential mass fractionation law so as to yield the <sup>40</sup>Ca/<sup>44</sup>Ca ratio of the SIL CaF<sub>2</sub> standard of 47.153 and the seawater ratio of 47.092. In essence, each measurement session reflects a new calibration of the double spike based on spiked analyses of these internal standards. Figure 11 records the long term pattern of adjustments made to the <sup>43</sup>Ca–<sup>42</sup>Ca ratio of the double-spike required to adjust for the instrumental drift. This is shown on the y-axis, on the right hand side of the diagram. The y-axis on the left hand side of the diagram shows the nominal per mil deviations in δ<sup>44</sup>Ca values that will result from these adjustments in spike composition. In other words, if the drift correction is not applied, the δ<sup>44</sup>Ca measurements of samples will drift in time by the amount shown on the left hand y-axis. Accordingly, if the drift is not carefully monitored and corrected for with standards, the long term reproducibility of δ<sup>44</sup>Ca is quite poor (±0.23‰, 2σ).

The best data is obtained for short sessions of about two weeks with 15–30 measurements completed, including standards. In the last 24 sessions, 41 <sup>44</sup>Ca/<sup>40</sup>Ca measurements of CaF<sub>2</sub> and 49 measurements of seawater were measured (excluding measurements whose δ values were sufficiently errant to warrant termination of the session). The average difference between the seawater and the CaF<sub>2</sub> standards is  $-1.29 \pm 0.03\text{‰}$  (2σ). The relatively low uncertainty benefits from taking the difference of averages of the two standards from each session, which minimizes the impact of outliers. A better sense of the reproducibility for a single measurement is estimated by taking the average standard deviation of 90 measurements of CaF<sub>2</sub> and seawater over the last 24 sessions, which combined yields  $\pm 0.07\text{‰}$  (2σ). The δ<sup>44</sup>Ca value of 915a measured over the same period is  $-1.86 \pm 0.05\text{‰}$  (2σ, n=13)



A close examination of Fig. 11 shows that the shift that occurred when the collectors were changed is not the largest shift observed over the recorded period. Therefore, swapping out the collectors does not solve the drift problem permanently. In addition, the shifts occur in both directions from the mean. Visual inspection of the graphite collectors removed from our machine showed that the formerly matte black collectors showed a luster over large areas (Fig. 12). The luster (which appears lighter or white in the photographs) is more prominent on one side of the collector than the other. Imaging of the original black and high luster areas of the collector using an electron microscope picked up no differences in elemental composition between them using an energy dispersive spectrometer, but differences in surface texture are visible (Fig. 13). The surfaces showing luster (white) are smoother than the original matte black areas of the collectors. We believe that the smoothing is caused by Ca ion beams hitting the sides of their respective collectors.

The angles of the collectors are factory set in order to optimize the collection of Nd isotopes, such that each ion beam in the Nd mass spectrum squarely impacts the back of its dedicated collector. Considering just four isotopes of Nd, the collector angles are optimized for a mass range of  $\sim 2.7\%$ . The same collectors used to measure four adjacent isotopes of Ca must accommodate a mass range of  $9.5\%$ . Consequently, the Ca ion beams hit the sides of their collectors, which may cause carbon to sputter from the low angles of interception, thus smoothing the surface of the collector over time. If the smoothing causes changes in collector efficiencies, then a physical explanation for the instrumental drift in Ca isotope measurements may have been found. But the smoothing phenomenon alone does not explain the fact that the drift is reversible (Fig. 11), unless the surface chemistry of the collector is also affected. We have noticed that the stability of the collector efficiencies is improved by running other elements into the collectors. The reason for this is unclear, but given the evidence for cup ablation in Fig. (12), and the interception of the Ca ion beams along the sides of the collectors, running other ions into the collectors might help to remove monolayers of calcium that may coat the surface of the collector

over long analysis sessions, or shorter sessions with large ion beam intensities, thus changing the surface insulating properties of the collector surface.

Although speculative, the hypothesis has merit because it helps to explain the improved reproducibility in  $\delta^{44}\text{Ca}$  that we obtain in the Saskatchewan Isotope Laboratory using a  $^{43}\text{Ca}$ – $^{42}\text{Ca}$  double spike coupled with dynamic collection, as compared to most other laboratories using  $^{48}\text{Ca}$ – $^{42}\text{Ca}$  or  $^{48}\text{Ca}$ – $^{43}\text{Ca}$  double spikes. Specifically, the  $^{43}\text{Ca}$ – $^{42}\text{Ca}$  double spike allows for a reduction in the integration time for the large  $^{40}\text{Ca}$  ion beam (presumably reducing the rate of build up of Ca ions on the collector surface), and a reduction in the angles of interception for all Ca ion beams with their respective collectors by restricting the mass range of measured Ca isotopes (i.e., increasing the depth of penetration of the ions into the collector). In addition, collecting the ion beams symmetrically with respect to the axial collector may reduce effects resulting from non-linear changes in ion optical properties across the image plane (Fletcher et al., 1997).

## REFERENCES

- Amini M., Eisenhauer A., Böhm F., Holmden C., Kreissig K., Hauff F., Jochum K. P. 2008. Calcium isotopes in MPI-DING Reference Glasses, USGS rock powders and various rocks: evidence for Ca isotope fractionation in terrestrial silicates. *Geostandards Newsletter* 33, 231–247.
- Bélanger N. and Holmden C. Apportionment study of Ca nutrition in a Boreal Shield forest of Saskatchewan (Canada) using  $^{87}\text{Sr}/^{86}\text{Sr}$  as a tracer, submitted to *Ecosystems*.
- Bishop, K. H., Grip, H. and O'Neill, A. (1990) The origins of acid runoff in a hillslope during storm events, *J. Hydrol.* 116, 35–61.
- Blum J. D. and Erel Y. (1997) Rb-Sr isotope systematics of a granitic soil chronosequence: The

- 857 importance of biotite weathering. *Geochim. Cosmochim. Acta* 61, 3193–3204.
- 858 Blum J. D., Klaue A., Nezat C. A., Driscoll C. T., Johnson C. E., Siccama T. G., Eagar C., Fahey  
859 T. J. and Likens G. E. (2002) Mycorrhizal weathering of apatite as an important Ca source  
860 in base-poor forest ecosystems. *Nature* 417, 729–731.
- 861 Bullen T. D., Fitzpatrick J. A., White A. F., Schulz M. S. and Vivit D. V. (2004) Calcium stable  
862 isotope evidence for three soil calcium pools at a granitoid chronosequence. In *Water-Rock*  
863 *Interaction, Proceedings of the Eleventh International Symposium on Water-Rock*  
864 *Interaction*, vol. 1 (eds. R. B. Wanty and R. R. Seal II). Taylor and Francis, London, pp.  
865 813–817.
- 866 Bullen T. D. and Bailey S. W. (2005) Identifying calcium sources at an acid deposition-impacted  
867 spruce forest: a strontium isotope, alkaline earth element multi-tracer approach.  
868 *Biogeochem.* 74, 63–99.
- 869 Buttle, J.M., Sami, K. (1992) Testing the groundwater ridging hypothesis of streamflow  
870 generation during snowmelt in a forested catchment. *J. Hydrol.* 135, 53–72.
- 871 Canadian National Atmospheric Chemistry Precipitation Database (1978-1992). Environment  
872 Canada, Meteorological Service of Canada, Toronto, ON.
- 873 Cenkci Tok B., Chabaux F., Lemarchand D., Schmitt A-D., Pierret M-C., Viville D., Bagard M-L.,  
874 Stille P. 2009. The impact of water-rock interaction and vegetation on calcium isotope  
875 fractionation in soil-and stream waters of a small, forested catchment (the Strengbach case).  
876 *Geochimica et Cosmochimica Acta* 73, 2215–2228.
- 877 Chadwick O. A., Derry L. A., Vitousek P. M., Huebert B. J. and Hedin L. O. (1999) Changing  
878 sources of nutrients during four million years of ecosystem development. *Nature* 397, 491–  
879 497.

- 880 DePaolo D. J. (2004) Calcium isotope variations produced by biological, kinetic, radiogenic, and  
881 nucleosynthetic processes. In *Geochemistry of Non-traditional Stable Isotopes* (eds. C. M.  
882 Johnson, B. L. Beard and F. Albarede). Reviews in Mineralogy, Mineralogical Society of  
883 America, Washington DC, pp. 255–288.
- 884 Dijkstra F. A. and Smits M. M. (2002) Tree species effects on calcium cycling: The role of  
885 calcium uptake in deep soils. *Ecosystems* 5, 385–398.
- 886 Drouet Th, Herbauts J., Gruber W. and Demaiffe D. (2005) Strontium isotope composition as a  
887 tracer of calcium sources in two forest ecosystems in Belgium. *Geoderma* 126, 203–23.
- 888 Eugster O., Tera F. and Wasserburg G. J. (1969) Isotopic analysis of barium in meteorites and in  
889 terrestrial samples. *J. Geophys. Res.* 74, 3897–3908.
- 890 Ewing S. A., Yang W., DePaolo D. J., Michalski G., Kendall C., Stewart B. W., Thiemens M.  
891 and Amundson R. (2008) Non-biological fractionation of stable Ca isotopes in the Atacama  
892 Desert, Chile. *Geochim. Cosmochim. Acta* 72, 1096–1110.
- 893 Fantle M.S. and DePaolo D.J. (2005) Variations in the marine Ca cycle over the past 20 million  
894 years. *Earth Planet. Sci. Lett.* 237, 102–117.
- 895 Fantle M. S. and DePaolo D. J. (2007) Ca isotopes in carbonate sediment and pore fluid from  
896 ODP Site 807A: The  $\text{Ca}^{2+}(\text{aq})$ -calcite equilibrium fractionation factor and calcite  
897 recrystallization in Pleistocene sediments. *Geochim. Cosmochim. Acta* 71, 2524–2546.
- 898 Fantle M. S. and Bullen T. D. (2009) Essentials of iron, chromium and calcium isotope analysis  
899 of natural materials by thermal ionization mass spectrometry. *Chem. Geol.* 258, 50–64.
- 900 Farkas J., Bohm F., Wallmann K., Blenkinsop J., Eisenhauer A., Geldren R. V., Munnecke A.,  
901 Voigt S. and Veizer J. (2007) Calcium isotope record of Phanerozoic oceans: Implications  
902 for chemical evolution of seawater and its causative mechanisms. *Geochim. Cosmochim.*  
903 *Acta* 71, 5117–134.

- 904 Fletcher I. R., Maggi A. L., Rosman K. J. R. and McNaughton N. J. (1997) Isotopic abundance  
905 measurements of K using a wide-dispersion multi-collector mass spectrometer and low-  
906 fractionation ionisation techniques. *Int. J. Mass Spectrom. Ion Proc.* 163, 1–17.
- 907 Gopalan K., Macdougall D. and Macissaac C. (2006) Evaluation of a Ca-42-Ca-43 double spike  
908 for high precision Ca isotope analysis. *International Journal of Mass Spectrometry* 248, 9-  
909 16.
- 910 Gussone N., Eisenhauer A., Heuser A., Dietzel M., Bock B., Bohm F., Spero H. J., Lea D. W.,  
911 Bijma J. and Nagler T. F. (2003) Model for kinetic effects on calcium isotope fractionation  
912 in inorganic aragonite and cultured planktonic foraminifera. *Geochim. Cosmochim. Acta*  
913 67, 1375–1382.
- 914 Gussone N., Bohm F., Eisenhauer A., Dietzel M., Heuser A., Teichert B. M. A., Reitner J.,  
915 Worheide G. and Dullo W-C. (2005) Calcium isotope fractionation in calcite and aragonite.  
916 *Geochim. Cosmochim. Acta* 69, 4485–4494.
- 917 Hart S. R. and Zindler A. (1989) Isotope fractionation laws – a test using calcium. *Int. J. Mass*  
918 *Spectrom. Ion Proc.* 89, 287–301.
- 919 Heuser A., Eisenhauer A., Gussone N., Bock B., Hansen B. T. and Nagler Th. F. (2002)  
920 Measurement of calcium isotopes ( $\delta^{44}\text{Ca}$ ) using a multicollector TIMS technique. *Int. J.*  
921 *Mass Spectrom.* 220, 385–397.
- 922 Hill, A.R. (2000) Stream chemistry and riparian zones In: Streams and Ground Waters, J.B. Jones  
923 and P.J. Mulholland (Eds). Academic Press, San Diego, CA. pp. 83–110.
- 924 Hippler D., Schmitt A.D., Gussone N., Heuser A., Stille P., Eisenhauer A. and Nagler T.F. (2003)  
925 Calcium isotopic composition of various reference materials and seawater. Geostandards  
926 Newsletter: The Journal of Geostandards and Geoanalysis 27, 13–19.
- 927 Holmden C. and Belanger N. (2006) Calcium isotope fractionation in a boreal forest ecosystem.  
928 *Geochim. Cosmochim. Acta* 70, (18) A261–A261 suppl. S, AUG–SEP.

- 929 Holmden C. (2005) Measurement of  $\delta^{44}\text{Ca}$  using a  $^{43}\text{Ca}$ – $^{42}\text{Ca}$  double-spike TIMS technique. In  
 930 *Summary of Investigations 2005*, Volume 1. Saskatchewan Geological Survey,  
 931 Saskatchewan Industry and Resources, Misc. Rep. 2005-1, CD-ROM, Paper A-4, 7p.
- 932 Hruska, J., Laudon, H., Johnson, C.E., Köhler, S., and Bishop, K. (2001) Acid/base character of  
 933 organic acids in a boreal stream during snowmelt. *Water Resources Research* 37, 1043–  
 934 1056.
- 935 Jacobson A. D. and Holmden C. (2008)  $\delta^{44}\text{Ca}$  evolution in a carbonate aquifer and its bearing on  
 936 the equilibrium isotope fractionation factor for calcite. *Earth Planet. Sci. Lett.* 270, 349–  
 937 353.
- 938 Jönsson C., Warfvinge P. and Sverdrup H. (1995) Application of the SAFE model to the Solling  
 939 spruce site. *Ecol. Model.* 83, 85–96.
- 940 Kalyn A. L. and Van Rees K. C. J. (2006) Contribution of fine roots to ecosystem biomass and  
 941 net primary production in blackspruce, aspen, and jack pine forests in Saskatchewan.  
 942 *Agricult. Forest Meteor.* 240, 236–243.
- 943 Kennedy M. J., Chadwick O. A., Vitousek P. M., Derry L. A. and Hendricks D. M. (1998)  
 944 Changing sources of base cations during ecosystem development, Hawaiian Islands.  
 945 *Geology* 26, 1015–1018.
- 946 Kennedy M. J., Hedin L. O. and Derry L. A. (2002) Decoupling of unpolluted temperate forest  
 947 from rock nutrient sources revealed by natural  $^{87}\text{Sr}/^{86}\text{Sr}$  and  $^{84}\text{Sr}$  tracer addition. *Proc. Natl.*  
 948 *Acad. Sci.* 99, 9639–9644.
- 949 Lemarchand D., Wasserburg G. J. and Papanastassiou D. A. (2004) Rate-controlled calcium  
 950 isotope fractionation in synthetic calcite. *Geochim. Cosmochim. Acta.* 68, 4665–4678.
- 951 Lambert M. C, Ung C. H. and Raulier F. (2005) Canadian national tree aboveground biomass  
 952 equations. *Can. J. For. Res.* 35, 1996–2018.
- 953 MacDonald J. D., Bélanger N., Sauvé S., Courchesne F. and Hendershot W. H. (2007) Collection

- 954 and characterization of soil solutions. In *Soil Sampling and Methods of Analysis* (eds. M.  
955 R. Carter and E. G. Gregorich), 2nd edition. CRC Press, Boca Raton.
- 956 McMartin I, Henderson P. J. and Nielsen E. (1999) Impact of a base metal smelter on the  
957 geochemistry of soils of the Flin Flon region, Manitoba and Saskatchewan. *Can. J. Earth*  
958 *Sci.* 36,141–160.
- 959 Miller H. G. (1995) The influence of stand development on nutrient demand, growth and  
960 allocation. *Plant Soil* 168, 225–232
- 961 Miller E. K., Blum J. D. and Friedland A. J. (1993) Determination of soil exchangeable-cation  
962 loss and weathering rates using Sr isotopes. *Nature* 362, 438–441.
- 963 Nezat C. A., Blum J. D., Yanai R. D. and Hamburg, S. P. (2007) A sequential extraction to  
964 determine the distribution of apatite in granitoid soil mineral pools with application to  
965 weathering at the Hubbard Brook Experimental Forest, NH, USA. *Appl. Geochem.* 22,  
966 2406–2421.
- 967 Obrien C. and Hendershot W. H. (1993) Separating streamflow into groundwater, solum and  
968 upwelling flow and its implications for hydrochemical modeling. *J. Hydrol.* 146, 1–12.
- 969 Page B. D., Bullen T. D. and Mitchell M. J. (2008) Influences of calcium availability and tree  
970 species on Ca isotope fractionation in soil and vegetation. *Biogeochem.* 88, 1–13.
- 971 Perakis S. S., Maguire D. A., Bullen T. D., Cromack K., Waring R. H. and Boyle J. R. (2006)  
972 Coupled nitrogen and calcium cycles in forests of the Oregon Coast Range. *Ecosystems* 9,  
973 63–74.
- 974 Russell W. A. and Papanastassiou D. A. (1978a) Ca isotope fractionation on the Earth and other  
975 solar system materials. *Geochim. Cosmochim. Acta* 42, 1075–1090.
- 976 Russell W. A. and Papanastassiou D. A. (1978b) Ca isotope fractionation in ion-exchange  
977 chromatography. *Analyt. Chem.* 50, 1151–1154.
- 978 Saskatchewan Environment (2006) [http://gisweb1.serm.gov.sk.ca/publicweb/Map\\_Gallery/Fire](http://gisweb1.serm.gov.sk.ca/publicweb/Map_Gallery/Fire)  
979 [/pdf/Historical\\_1945\\_2006.pdf](http://gisweb1.serm.gov.sk.ca/publicweb/Map_Gallery/Fire/pdf/Historical_1945_2006.pdf)

- 980 Schmit A-D., Chabaux F. and Stille P. (2003) The calcium riverine and hydrothermal isotopic  
981 fluxes and the oceanic calcium mass balance. *Earth Planet. Sci. Lett.*, 213, 503–518.
- 982 Schmitt A-D. and Stille P. (2005) The source of calcium in wet atmospheric deposits: Ca-Sr  
983 isotope evidence. *Geochim. Cosmochim. Acta* 69, 3463–3468.
- 984 Skulan J. L., De Paolo D. J. and Owens T. L. (1997) Biological control of calcium isotopic  
985 abundances in the global calcium cycle. *Geochim. Cosmochim. Acta* 61, 2505–2510.
- 986 Sime N. G., De La Rocha C. L. and Galy A. (2005) Negligible temperature dependence of  
987 calcium isotope fractionation in 12 species of planktonic foraminifera. *Earth Planet. Sci.*  
988 *Lett.* 232, 51–66.
- 989 Steuber T. and Buhl D. (2006) Calcium-isotope fractionation in selected modern and ancient  
990 marine carbonates. *Geochim. Cosmochim. Acta* 70, 5507–5521.
- 991 Stewart B. W., Capo R. C. and Chadwick O. A. (1998) Quantitative strontium isotope models for  
992 weathering, pedogenesis and biogeochemical cycling. *Geoderma* 82, 173–195.
- 993 Sverdrup H. U. (1990) *The kinetics of base cation release due to chemical weathering*. Lund  
994 University Press, Lund, Sweden, 246 p.
- 995 Sverdrup H. and Warfvinge P. (1995) Critical loads of acidity for Swedish forest ecosystems.  
996 *Ecol. Bull.* 44, 75–89.
- 997 Tipper E.T., Galy A. and Bickle M.J. (2006) Riverine evidence for a fractionated reservoir of Ca  
998 and Mg on the continents: Implications for the oceanic Ca cycle. *Earth Planet. Sci. Lett.*  
999 247, 267–279.
- 1000 Upadhyay D., Scherer E. E. and Mezger K (2008) Fractionation and mixing of Nd isotopes  
1001 during thermal ionization mass spectrometry: implications for high precision  $^{142}\text{Nd}/^{144}\text{Nd}$   
1002 analyses. *J. Analyt. Atom. Spectrom.* 23, 561–568.
- 1003 Wiegand B. A, Chadwick O. A., Vitousek P. M. and Wooden J. L. (2005) Ca cycling and isotopic  
1004 fluxes in forested ecosystems in Hawaii. *Geophys. Res. Lett.* 32, L11404. Doi:  
1005 10.1029/2005GLO22746.



Yin X. and Arp P. A. (1993) Predicting forest soil temperatures from monthly air temperature and precipitation records. *Can. J. For. Res.* 23, 2521–2536.

Zhu P. and MacDougall J. D. (1998) Calcium isotopes in the marine environment and the oceanic calcium cycle. *Geochim. Cosmochim. Acta* 62, 1691–1698.

## Figure Captions

Fig. 1. Map of Saskatchewan, Canada, showing the location of the study area in relation to ecozones and population centers. Sites identified with the target symbol are locations where Ca has been measured in wet deposition by Environment Canada (see Fig. 7).

Fig. 2. Schematic illustration of the topography of Toposequence 1 in the Boreal Shield study site near La Ronge, Saskatchewan, showing the first order stream, study plot locations, soil types, and major tree species. Shown are  $\delta^{44}\text{Ca}$  values for vegetation, soil pools, groundwater, granite bedrock, seasonally averaged precipitation, and the average value for eight measurements of the stream taken from the 2005 field season. Two  $\delta^{44}\text{Ca}$  values for each tree are shown: the upper value represents foliage; the lower value represents stemwood. This toposequence supports a mixedwood forest.

Fig. 3. Schematic illustration of the topography of Toposequence 2, located 40 m upstream from Toposequence 1. Shown are  $\delta^{44}\text{Ca}$  values for vegetation and soil pools (see Fig. 2 for additional information). This toposequence supports a black spruce/feathermoss forest.

Fig. 4. Two-box model of the forest Ca cycle highlighting the impact of atmospheric deposition, soil mineral weathering, and plant uptake on the isotope balance of Ca in the plant available Ca

pools of the forest floor and upper B horizon. Soil depth thickness of each Ca pool is also shown.

Model parameters and system components are defined in Table 1.

Fig. 5. Relationship between  $\delta^{44}\text{Ca}$  values in stemwood and foliage samples collected from the six study plots. The y-intercept gives a sense of the magnitude of the Ca isotope fractionation between foliage and stemwood.

Fig. 6. Plot of  $^{87}\text{Sr}/^{86}\text{Sr}$  vs.  $\delta^{44}\text{Ca}$  for extracts and acid leaches of lower B/C mineral soils from each study plot. The acid leaches were performed in order to determine the Sr and Ca isotope compositions of the soil mineral weathering end-member. The paths joining sample points reflect (from right to left) the sequential treatments applied to each soil sample in the following order: 0.1 N  $\text{BaCl}_2$ –1 N  $\text{HNO}_3$ –15 N  $\text{HNO}_3$ . The  $^{87}\text{Sr}/^{86}\text{Sr}$  ratios increase and  $\delta^{44}\text{Ca}$  values decrease with increasing strength of treatment. The  $\delta^{44}\text{Ca}$  trends appear to reach plateau values of either  $-1.06$  or  $-1.16\text{‰}$  (gray bands) that additional leaching is unlikely to change. By contrast,  $^{87}\text{Sr}/^{86}\text{Sr}$  ratios steadily increase with each successively more aggressive treatment, indicating fractional increases in the Sr contributions from biotite and possibly K-feldspar.

Fig. 7. Measurements of Ca in wet deposition from three sites in Saskatchewan (Canadian National Atmospheric Chemistry Precipitation Database (1978-1992)). The dashed line indicates the seasonally averaged wet deposition flux of Ca at the La Ronge study site ( $0.0024 \text{ mol Ca m}^{-2} \text{ y}^{-1}$ ) measured from data collected as part of this study.

Fig. 8. The initial steady state  $\delta^{44}\text{Ca}$  values for plot 1.1 are shown to the left of the diagram for the forest floor and upper B soil pools. The  $\delta^{44}\text{Ca}$  value of the vegetation is also shown. An increase of 50% in the Ca uptake flux causes the  $\delta^{44}\text{Ca}$  values of both soil vegetation pools to

increase as the system adjusts to the new steady state condition. The time needed to reach steady state is a function of the mass of Ca in the soil pools.

Fig. 9. The initial steady state  $\delta^{44}\text{Ca}$  values for plot 1.1 are shown to the left of the diagram for the forest floor and upper B soil pools. The  $\delta^{44}\text{Ca}$  value of the vegetation is also shown. The initial steady state was perturbed in two ways: forest productivity (the Ca uptake rate) was increased by 1.4 times, and the species specific Ca isotope fractionation factor ( $\Delta_{\text{soil}}^{\text{veg}}$ ) was increased 2.8 times. The new steady state condition is characterized by lower  $\delta^{44}\text{Ca}$  values in vegetation and a more dramatic  $\delta^{44}\text{Ca}$  gradient with soil depth. The shift in the forest floor Ca pool towards lower  $\delta^{44}\text{Ca}$  values reflects the interplay between increased Ca uptake rate and decreased  $\delta^{44}\text{Ca}$  of litterfall caused by the increase in the fractionation factor.

Fig. 10. Faraday collector configuration used for Ca isotope measurements. The duty cycle consists of three mass scans. Isotope masses are collected symmetrically with respect to the axial collector. Signal integration times are given in parentheses in units of seconds (s).

Fig. 11. Plot showing the range in instrumental drift of the Triton instrument over a three-year period. The magnitude of the drift is quantified by monitoring adjustments made to the  $^{43}\text{Ca}$ – $^{42}\text{Ca}$  ratio of the double spike (using an exponential law) required to negate the effect of the drift on the reproducibility of the ‘absolute’  $^{44}\text{Ca}/^{40}\text{Ca}$  ratios of the  $\text{CaF}_2$  and seawater standards. If the drift is not corrected for, then the long-term reproducibility is poor (on the order of  $\pm 0.23\%$  ( $2\sigma$ )). On the other hand, the reproducibility is much improved ( $\pm 0.065\%$ ,  $2\sigma$ ) if a drift correction is applied by closely monitoring the standards. Instrumental drift, however, is not the only factor that influences the external precision of the measurements. Reproducible loading, focusing, and mass fractionation during the run are also important. When these additional factors

are tightly controlled, the reproducibility ultimately rests on the analyst's ability to recognize and correct for effects of instrumental drift. To validate our approach, 13 measurements of SRM 915a were performed at least once in 13 different sessions over the past two years, yielding  $-1.86 \pm 0.05\text{‰}$  ( $2\sigma$ ). Although the instrumental drift was  $\sim 0.3\text{‰}$  over this period, the measurements of 915a fall within a total range of  $0.1\text{‰}$ , at the 95% confidence level. A similar drift correction could be made by normalization to a sequence of standards run at the same time as a sequence of samples.

Fig. 12. Original (factory installed in 2002) L2 Faraday collector graphite inserts from the SIL Triton instrument used to collect  $^{40}\text{Ca}$  according to the collector configuration in Holmden (2005). The graphite inserts for eight moveable collectors were replaced October 6, 2006. Most of the collectors showed a luster over large areas of their surfaces (the lighter or whiter areas in the photographs). New collectors show a matte black appearance in reflected light.

Fig. 13. Electron microscopy image of the L2 collector. A. The black areas of the collector seen in Fig. 12 have rough surfaces; the white areas have smooth surfaces. The white areas are where the ion beams hit the collector (Magnification is 250 times). B. Close-up image of the white area in 13A, showing altered smooth surface of collector (2500 times). C. Close-up image of the black area in 13A showing original rough surface of collector (2500 times). D. Close-up image of the transitional area between smooth and rough textured surfaces found along the inner edge of the collector.

Table 1. Definitions for model variables and system components

Variables	Description	Units
$M_i$	moles of Ca in component i per unit area	$\text{mol m}^{-2}$
$f_i$	flux density of Ca for component i	$\text{mol m}^{-2} \text{y}^{-1}$
$\delta_i$	$\delta^{44}\text{Ca}$ value of component i	‰
$\Delta_{i1}^{i2}$	fractionation factor between components 1 and 2	‰
$X$	fraction of Ca taken up by fine roots in forest floor compared to upper B horizon	
Components ( <i>i</i> )		
veg	trees	
FF	forest floor	
B	upper B horizon permeated by fine roots	
soil	combined forest floor and upper B soil pools	
stem	stemwood	
foliage	foliage	
B/C	lower B horizon (BC) below finely rooted soil	
a	atmospheric deposition	
w	weathering	
lf	litterfall	
u	plant uptake	
z	leach loss from forest floor	
gw	leach loss to groundwater	

Table 2. Ca and Sr isotopic and elemental data for the La Ronge watershed

Sample Description	$\delta^{44}\text{Ca}$ (‰ seawater)	2 s.e.	Ca (ppm)	$^{87}\text{Sr}/^{86}\text{Sr}^1$
<b>Precipitation</b>				
<b>Summer —open field (above canopy)</b>				
BP3 July 6/05	-1.31	0.04	0.496	—
BP3 July 14/05	—	—	0.472	—
BP3 July 30/05	-1.31	0.05	0.168	—
Average	-1.31	—	0.379	—
<b>Snow pack</b>				
Nemeiben Lake 1	-1.21	0.05	0.135	—
Nemeiben Lake 2	-1.20	0.05	0.212	—
Lac La Ronge 1	-1.41	0.04	0.178	—
Lac La Ronge 2	-1.25	0.04	0.195	—
Average	-1.22	—	0.180	—
<b>Average Precipitation</b> (30%) and rain (70%)	-1.28	—	0.319	—
<b>Toposequence 1</b>				
<b>Plot 1.1</b>				
<b>Foliage</b>				
Jack Pine	-0.64	0.06	6285	—
Trembling Aspen	-1.30	0.05	12703	—
Black Spruce (young)	-1.07	0.04	6254	—
Black Spruce (old)	-1.20	0.04	10071	—
<b>Stemwood</b>				
Jack Pine	-1.14	0.06	1268	—
Trembling Aspen	-1.79	0.04	3274	—
Black Spruce (old)	-1.58	0.05	1761	—
<b>Roots</b>				
Jack Pine 2.0 mm	-1.57	0.05	3053	—
Trembling Aspen 2.0 mm	-2.18	0.10	4166	—
<b>Soil pools (lysimeters)</b>				
Forest floor horizon (~10 cm depth)	-1.02	0.04	6.40	—
Upper B horizon (~35 cm depth)	-0.79	0.05	—	—
<b>Extracts and acid leaches (B/C horizon, 50–65 cm depth)</b>				
BaCl <sub>2</sub>	-0.80	0.03	41.1	0.7143
1N HNO <sub>3</sub>	-1.14	0.04	314	0.7155
15N HNO <sub>3</sub>	-1.05	0.05	629	0.7394
Residue	—	—	—	0.7074
<b>Plot 1.2</b>				
<b>Foliage</b>				
jack Pine	-0.65	0.07	6794	—
trembling Aspen	-0.96	0.04	15443	—
black Spruce (young)	-1.31	0.06	7742	—
black Spruce (old)	-1.24	0.05	3748	—
<b>Stemwood</b>				
jack Pine	-1.19	0.05	1001	—
trembling Aspen	-1.44	0.06	1915	—
black Spruce (old)	-1.68	0.05	1894	—
<b>Roots</b>				
trembling Aspen 0.5 mm	-1.26	0.04	2593	—
trembling Aspen 2.0 mm	-2.03	0.03	4769	—
black Spruce 2.0 mm	-2.11	0.04	—	—
<b>Soil pools (lysimeters)</b>				
Forest floor horizon (~10 cm depth)	-1.05	0.05	16.6	—
Upper B horizon (~35 cm depth)	-0.69	0.06	6.23	—
<b>Extracts and acid leaches (B/C horizon, 50–65 cm depth)</b>				
BaCl <sub>2</sub>	-0.56	0.04	117	0.7112
1N HNO <sub>3</sub>	-0.95	0.04	604	0.7327
15N HNO <sub>3</sub>	-1.06	0.04	829	0.7497
residue	—	—	—	0.7070
<b>Plot 1.3</b>				
<b>Foliage</b>				
trembling Aspen	-0.89	0.04	13612	—
black Spruce (young)	-1.34	0.05	6050	—
black Spruce (old)	-1.31	0.05	11030	—
white Spruce	-1.32	0.05	12911	—
balsam Poplar	-0.90	0.04	13684	—
<b>Stemwood</b>				
trembling Aspen	-1.40	0.04	2120	—
black Spruce (old)	-1.60	0.06	1658.25	—
white Spruce	-1.64	0.04	995.00	—
balsam Poplar	-1.65	0.04	4987	—
<b>Soil pools (lysimeters)</b>				
Forest floor horizon (~10 cm depth)	-0.85	0.04	7.46	—
Ah (~20 cm depth)	-0.55	0.06	7.58	—
Upper B horizon (~35 cm depth)	-0.45	0.03	10.22	—
<b>Groundwater</b>				
1.4m	-0.57	0.10	13.17	—
1.8 m	-0.60	0.06	27.53	—
<b>Extracts and acid leaches (B/C horizon, 50–65 cm depth)</b>				
BaCl <sub>2</sub>	-0.68	0.03	2393	0.7354
1N HNO <sub>3</sub>	-0.81	0.03	1233	0.7471
15N HNO <sub>3</sub>	-1.14	0.04	1455	0.7774
residue	—	—	—	0.7240

1. See Bélanger and Holmden (submitted) for complete  $^{87}\text{Sr}/^{86}\text{Sr}$  dataset

Table 2. (continued)

Sample Description	$\delta^{44}\text{Ca}$ (‰ seawater)	2 s.e.	Ca (ppm)	$^{87}\text{Sr}/^{86}\text{Sr}^1$
<b>Toposequence 2</b>				
<b>Plot 2.1</b>				
<b>Foliage</b>				
Black spruce - a	-1.27	0.04	16756	—
Black spruce - b	-1.04	0.04	9471	—
<b>Stemwood</b>				
Black spruce - b	-1.26	0.04	924	—
<b>Roots</b>				
Black Spruce 2.0 mm	-2.11	0.04	4868	—
<b>Soil pools (lysimeters)</b>				
Forest floor horizon (~10 cm depth)	-1.03	0.04	7.71	—
Upper B horizon (~35 cm depth)	-0.88	0.04	6.55	—
<b>Extracts and acid leaches (B/C horizon, 50–65 cm depth)</b>				
BaCl <sub>2</sub>	-0.84	0.03	1445	0.7224
1N HNO <sub>3</sub>	-0.95	0.03	713	0.7370
15N HNO <sub>3</sub>	-1.17	0.03	1521	0.7943
residue	—	—	—	0.7176
<b>Plot 2.2</b>				
<b>Foliage</b>				
Black spruce - a	-1.43	0.06	7883	—
Black spruce - b	-1.22	0.04	7841	—
Jack pine	-0.38	0.06	3487	—
<b>Stemwood</b>				
Black spruce - b	-1.81	0.04	1020	—
jack pine	-0.89	0.04	782	—
<b>Roots</b>				
Black Spruce 2.0 mm	-2.20	0.03	3687	—
jack Pine	-1.54	0.04	2145	—
<b>Soil pools (lysimeters)</b>				
Forest floor horizon (~10 cm depth)	-0.83	0.04	3.59	—
Upper B horizon (~35 cm depth)	-0.78	0.07	2.80	—
<b>Extracts and acid leaches (B/C horizon, 50–65 cm depth)</b>				
BaCl <sub>2</sub>	-0.94	0.03	231	0.7147
1N HNO <sub>3</sub>	-1.15	0.04	903	0.7363
15N HNO <sub>3</sub>	-1.16	0.03	1107	0.8229
residue	—	—	—	0.7122
<b>Plot 2.3</b>				
<b>Foliage</b>				
Black spruce - a	-1.28	0.07	10071	—
Black spruce - b	-1.43	0.04	10355	—
<b>Stemwood</b>				
Black spruce - b	-1.65	0.04	1356	—
<b>Soil pools (lysimeters)</b>				
Forest floor horizon (~10 cm depth)	-0.91	0.03	5.63	—
Ah (~20 cm depth)	-0.90	0.03	6.03	—
Upper B horizon (~35 cm depth)	-0.81	0.06	5.90	—
<b>Groundwater</b>				
1.4m	-0.80	0.06	8.39	—
1.8 m	-0.69	0.07	17.14	—
<b>Extracts and acid leaches (B/C horizon, 50–65 cm depth)</b>				
BaCl <sub>2</sub>	-0.91	0.03	1234	0.7297
1N HNO <sub>3</sub>	-0.91	0.03	1159	0.7392
15N HNO <sub>3</sub>	-1.18	0.06	1909	0.7730
residue	—	—	—	0.7150
<b>Other</b>				
<b>Streamwater</b>				
15-Jul	-0.70	0.03	4.81	—
23-Jun	-0.65	0.05	4.38	—
1-Jul	-0.59	0.05	4.22	—
7-Jul	-0.55	0.06	4.55	—
31-Jul	-0.58	0.05	5.48	—
1-Sep	-0.53	0.05	5.07	—
21-Sept	-0.63	0.06	5.65	—
19-Oct	-0.63	0.06	4.70	—
<b>Granite</b>				
Bulk	-1.27	0.04	19022	0.7089
1 N HNO <sub>3</sub> Leach	-1.36	0.05	—	0.7152
15 N HNO <sub>3</sub> Leach	-1.57	0.04	—	0.8950
Corrected for $^{87}\text{Sr}$ growth (Rb = 43 ppm)	—	—	—	0.7068
<b>Potted plant</b>				
Basalt	-0.88	0.05	—	—
root (radicle)	-1.30	0.05	—	—
root (secondary)	-1.29	0.06	—	—
stem	-1.38	0.05	—	—
leaf	-0.52	0.08	—	—

1. See Bélanger and Holmden (submitted) for complete  $^{87}\text{Sr}/^{86}\text{Sr}$  dataset

Table 3. Separation factors describing the distribution of  $\delta^{44}\text{Ca}$  between trees and soil pools by species

Tree	Plot	Stem	Foliage	Roots 2.0 mm	stem-FF <sup>1</sup>	stem-B <sup>2</sup>	stem-B/C <sup>3</sup>	foliage-stem	stem-root
<i>separation factors</i>									
t. aspen	1.1	-1.79	-1.30	-2.18	-0.77	-1.00	-0.99	0.49	0.39
t. aspen	1.2	-1.44	-0.96	-2.03	-0.39	-0.75	-0.88	0.48	0.43
t. aspen	1.3	-1.40	-0.89	—	-0.55	-0.85	-0.72	0.51	—
				mean	-0.57	-0.85	-0.86	0.49	0.41
				s.e.	0.11	0.07	0.08	0.01	0.02
j. pine	1.1	-1.14	-0.64	-1.57	-0.12	-0.35	-0.34	0.50	0.43
j. pine	1.2	-1.19	-0.65	n.d.	-0.14	-0.50	-0.63	0.54	—
j. pine	2.2	-0.89	-0.38	—	-0.06	-0.11	0.05	0.51	—
				mean	-0.11	-0.32	-0.31	0.52	0.43
				s.e.	0.02	0.11	0.20	0.01	—
b. spruce	1.1	-1.58	-1.20	—	-0.56	-0.79	-0.78	0.38	—
b. spruce	1.2	-1.68	-1.24	-2.11	-0.63	-0.99	-1.12	0.44	0.43
b. spruce	1.3	-1.60	-1.31	0.00	-0.75	-1.05	-0.92	0.29	—
b. spruce <sup>4</sup>	2.1	-1.26	-1.04	—	-0.23	-0.38	-0.42	0.22	—
b. spruce	2.2	-1.81	-1.22	-2.2	-0.98	-1.03	-0.87	0.59	0.39
b. spruce	2.3	-1.65	-1.43	—	-0.74	-0.75	-0.74	0.22	—
				mean	-0.73	-0.92	-0.89	0.36	0.41
				s.e.	0.16	0.14	0.15	0.14	0.03
Grand mean (spruce and aspen)					-0.67	-0.90	-0.88		
Grand mean (all species)					0.18	0.13	0.13		
								0.43	0.41
								0.12	0.02

1. FF = Ca from FF soil solution collected using lysimeter

2. B = Ca from upepr B soil solution collected using lysimeter

3. B/C = Ca from BaCl<sub>2</sub> extract of B/C horizon4. Plot 2.1 stemwood  $\delta^{44}\text{Ca}$  not included in averages or grand mean.



Table 4. Ca in soil and vegetation pools and weighted  $\delta^{44}\text{Ca}$  values

Type	Sampled Depth (cm)	$f_u^4$ (mol m <sup>-2</sup> y <sup>-1</sup> )	Ca pools <sup>1</sup> (mol m <sup>-2</sup> )	$\delta^{44}\text{Ca}$ (‰)	$f_u^4$ (mol m <sup>-2</sup> y <sup>-1</sup> )	Ca pools <sup>1</sup> (mol m <sup>-2</sup> )	$\delta^{44}\text{Ca}$ (‰)
<b>Vegetation</b>		<b>Plot 1.1</b>		<b>Plot 2.1</b>			
Stem <sup>2</sup>			0.832	-1.60		0.92	-1.25
Foliage			0.267	-1.18		0.66	-1.15
Roots <sup>3</sup>			0.197	-1.63		0.22	-1.30
Plot avg. (weighted)		0.0549	1.30	-1.52	0.0939	1.80	-1.22
<b>Soil pools</b>							
Forest floor	10		0.1623	-1.02		1.00	-1.03
Upper B	35		0.1185	-0.79		6.55	-0.88
B/C	50–65			-0.80			-0.84
<b>Vegetation</b>		<b>Plot 1.2</b>		<b>Plot 2.2</b>			
Stem <sup>2</sup>			1.128	-1.54		0.73	-1.81
Foliage			0.315	-1.20		0.56	-1.33
Roots <sup>3</sup>			0.215	-1.57		0.17	-1.82
Plot avg. (weighted)		0.0808	1.66	-1.48	0.0794	1.45	-1.63
<b>Soil pools</b>							
Forest floor	10		0.8705	-1.05		0.31	-0.83
Upper B	35		0.4840	-0.85		1.47	-0.78
B/C	50–65			-0.56			-0.94
<b>Vegetation</b>		<b>Plot 1.3</b>	<b>Plot 1.3</b>	<b>Plot 2.3</b>			
Stem <sup>2</sup>			0.996	-1.63		1.51	-1.65
Foliage			0.611	-1.32		0.56	-1.36
Roots <sup>3</sup>			0.344	-1.66		0.30	-1.67
Plot avg. (weighted)		0.0873	1.95	-1.54	0.1097	2.38	-1.58
<b>Soil pools</b>							
Forest floor	10		1.228	-0.85		1.52	-0.91
Ah	20		3.202	-0.55		2.61	-0.90
Upper B	35		4.576	-0.45		5.480	-0.81
B/C	50–65			-0.68			-0.91

1. Soil Ca pools based BaCl<sub>2</sub> technique. Vegetation pools determined using allometric equations of Lambert et al. (2005).

2. Stem Ca pool consists of stemwood, branches, and bark.

3. Root Ca concentration estimated by method described in Bélanger and Holmden (submitted).

4. Ca uptake flux calculated as the yearly flux of Ca needed to replace foliage (see text for explanation).

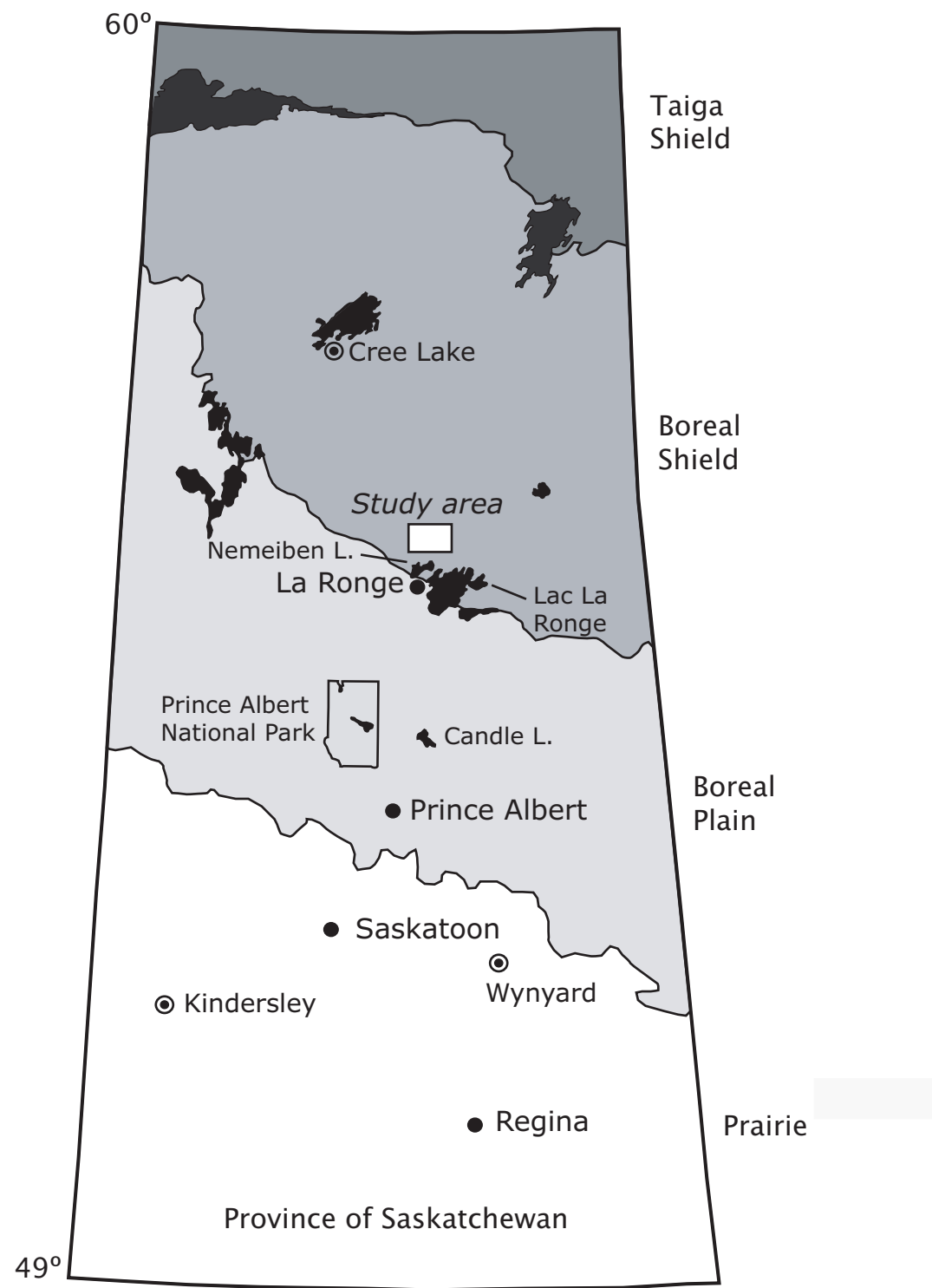
Table 5. Principal inputs and modeled Ca fluxes and fractionation factors for each plot using steady state equations.

Plot	$\Delta_{soil}^{veg1}$	$X$	$f_a$	$\delta_{lf}$	$\left( \frac{Ca_a}{Ca_a + Ca_w} \right)_{veg}^2$	$f_{lf}$	$f_z$	$f_w$	$f_{gw}$
	‰		mol m <sup>-2</sup> y <sup>-1</sup>	‰		mol m <sup>-2</sup> y <sup>-1</sup>	mol m <sup>-2</sup> y <sup>-1</sup>	mol m <sup>-2</sup> y <sup>-2</sup>	mol m <sup>-2</sup> y <sup>-1</sup>
			—output—			—output—			
1.1	-0.611	0.52	0.0180	-1.18	0.94	0.0784	0.0677	0.0016	0.0431
1.2	-0.530	0.50	0.0175	-1.20	0.62	0.1131	0.0904	0.0165	0.0663
1.3	-0.839	0.63	0.0125	-1.32	0.56	0.0865	0.0443	0.0138	0.0255
2.1	-0.239	0.67	0.0185	-1.15	0.91	0.0861	0.0420	0.0043	0.0151
2.2	-0.809	0.78	0.0110	-1.33	0.77	0.0896	0.0391	0.0337	0.0550
2.3	-0.701	0.74	0.0110	-1.36	0.55	0.1168	0.0470	0.0453	0.0634
Average	-0.70	0.64	0.015			0.095	0.055	0.019	0.045
1 $\sigma$	0.13	0.12	0.003			0.016	0.020	0.017	0.021

1. Average does not include the fractionation factor from plot 2.1.

2. Apportioning of Ca between atmospheric deposition and soil mineral weathering sources in vegetation using <sup>87</sup>Sr/<sup>86</sup>Sr as a tracer (Bélanger and Holmden, submitted).

Figure 1



**Fig.2**  
Holmden and Bélanger

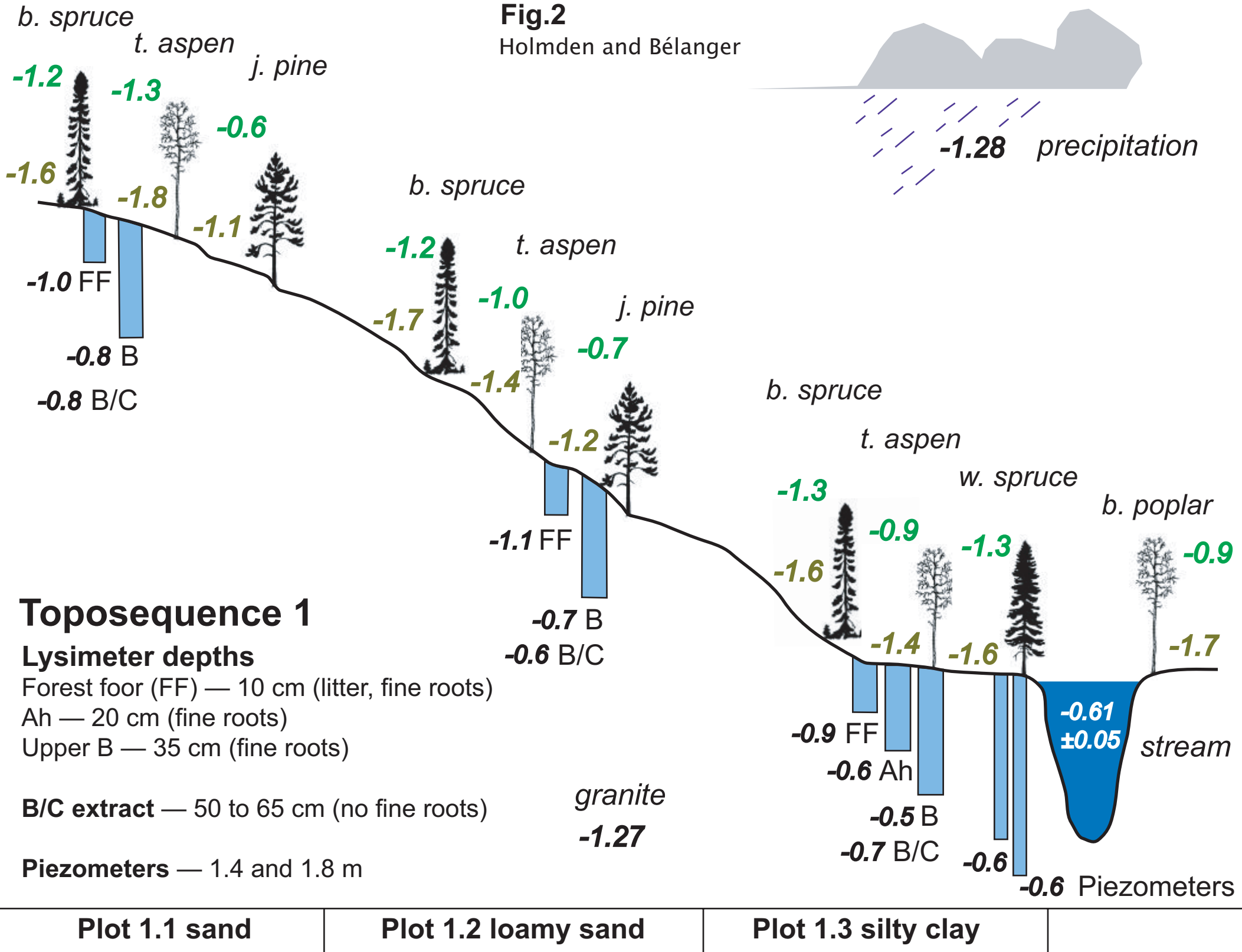
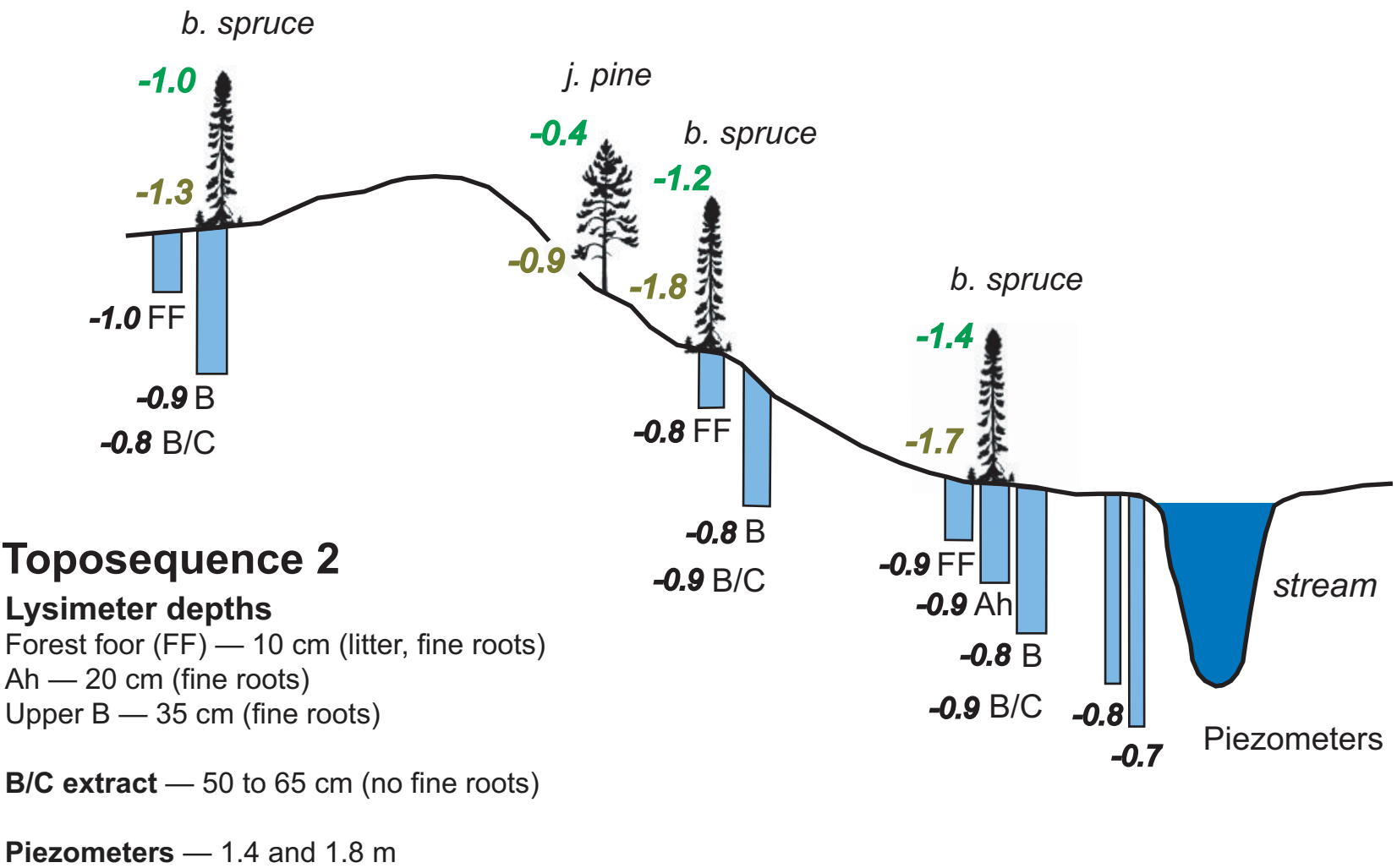
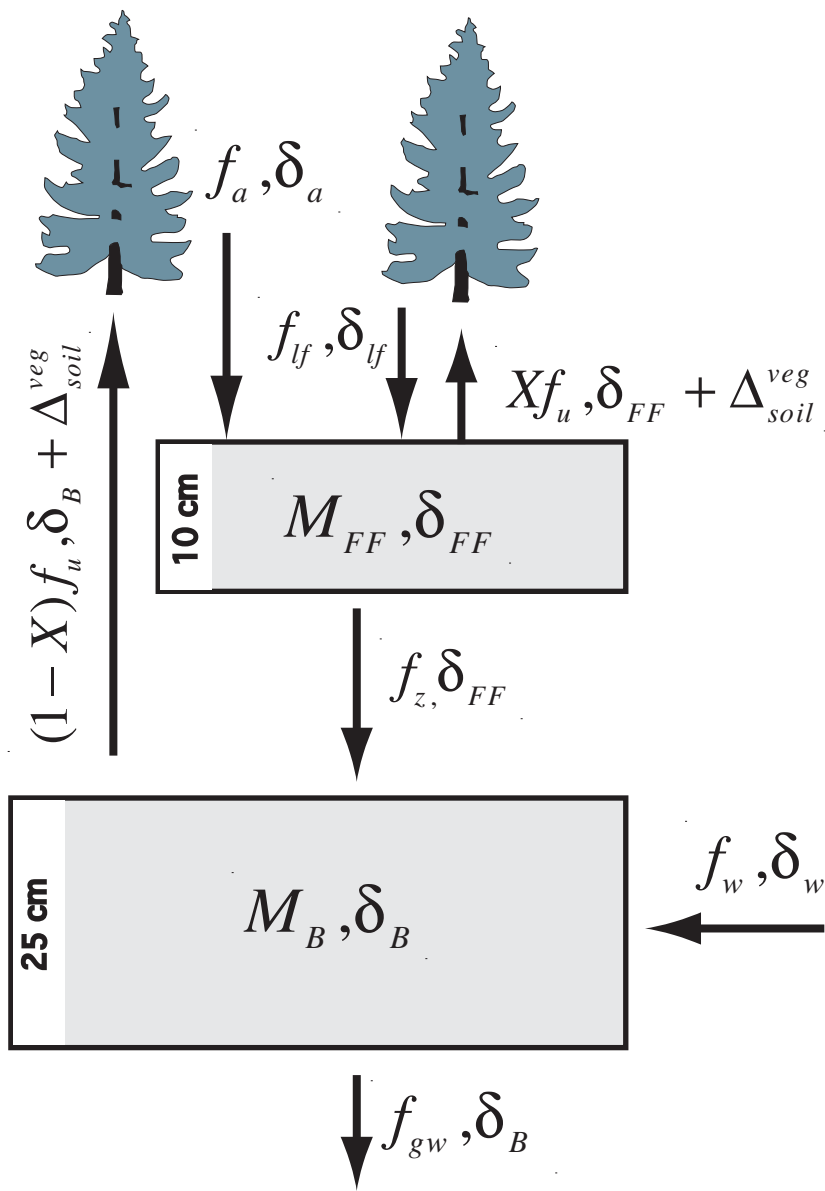


Fig. 3

Holmden and Bélanger

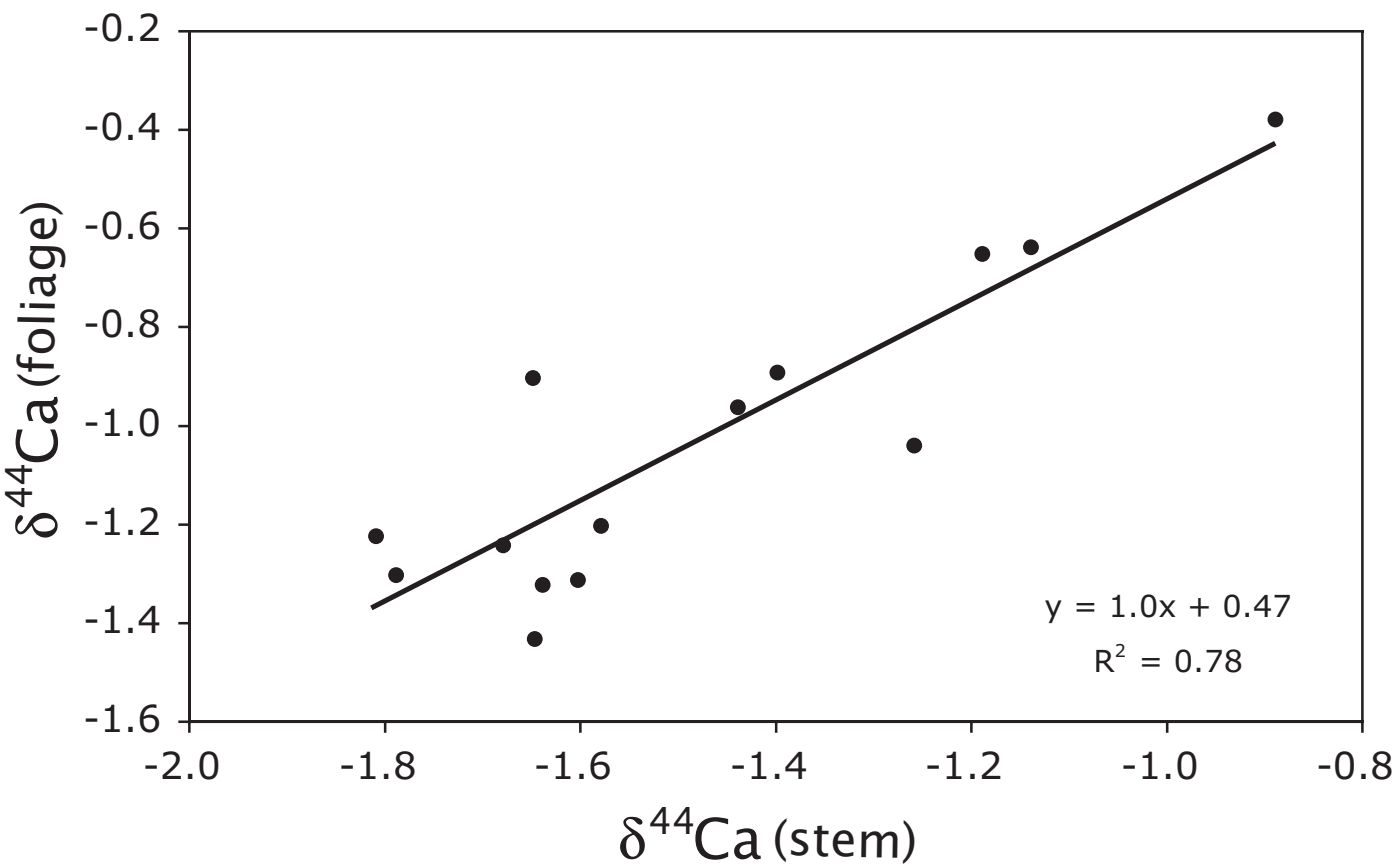


**Fig. 4**



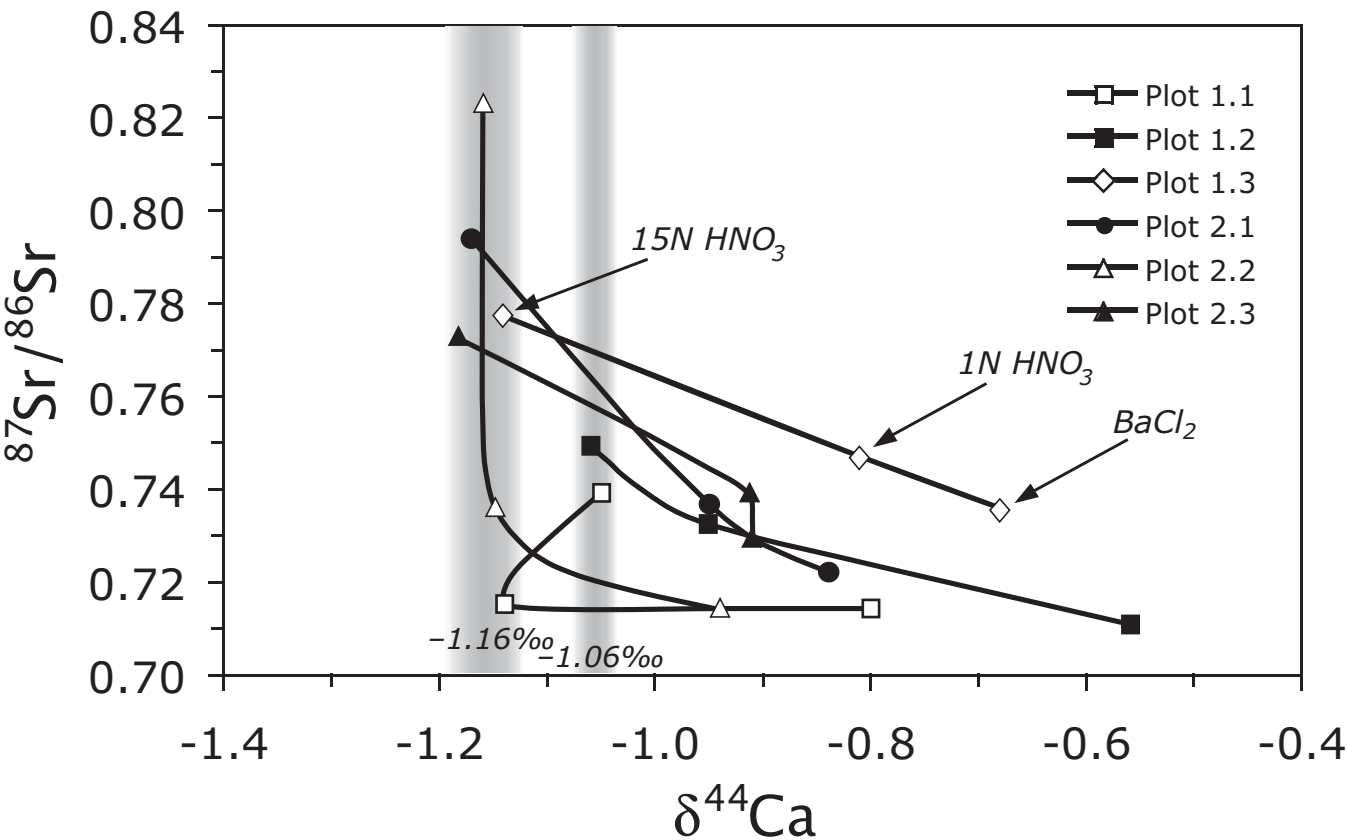
**Fig. 5**

Holmden and Bélanger



**Fig. 6**

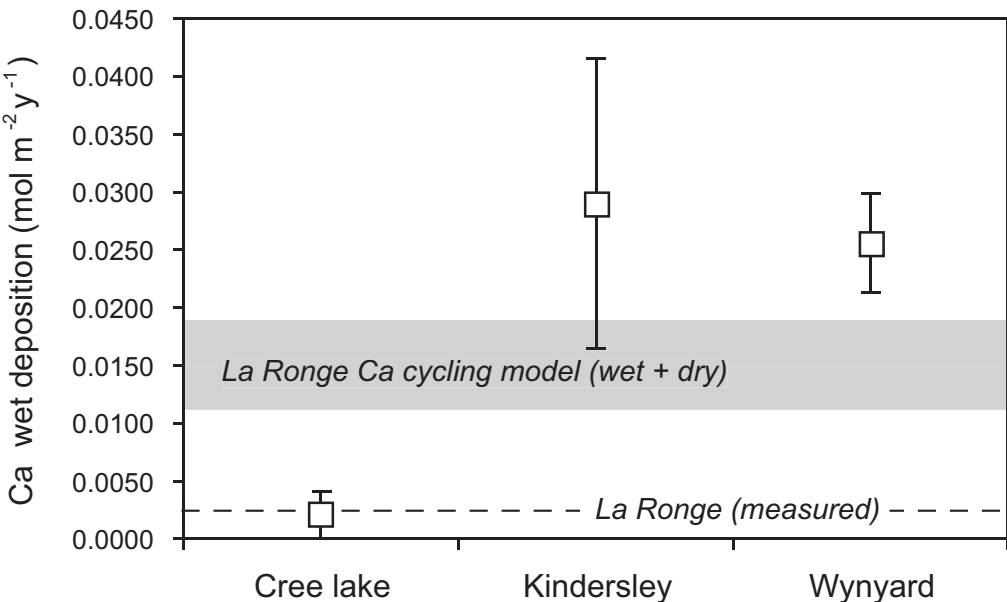
Holmden and Bélanger





**Fig. 7**

Holmden and Bélanger



**Fig. 8**

Holmden and Bélanger

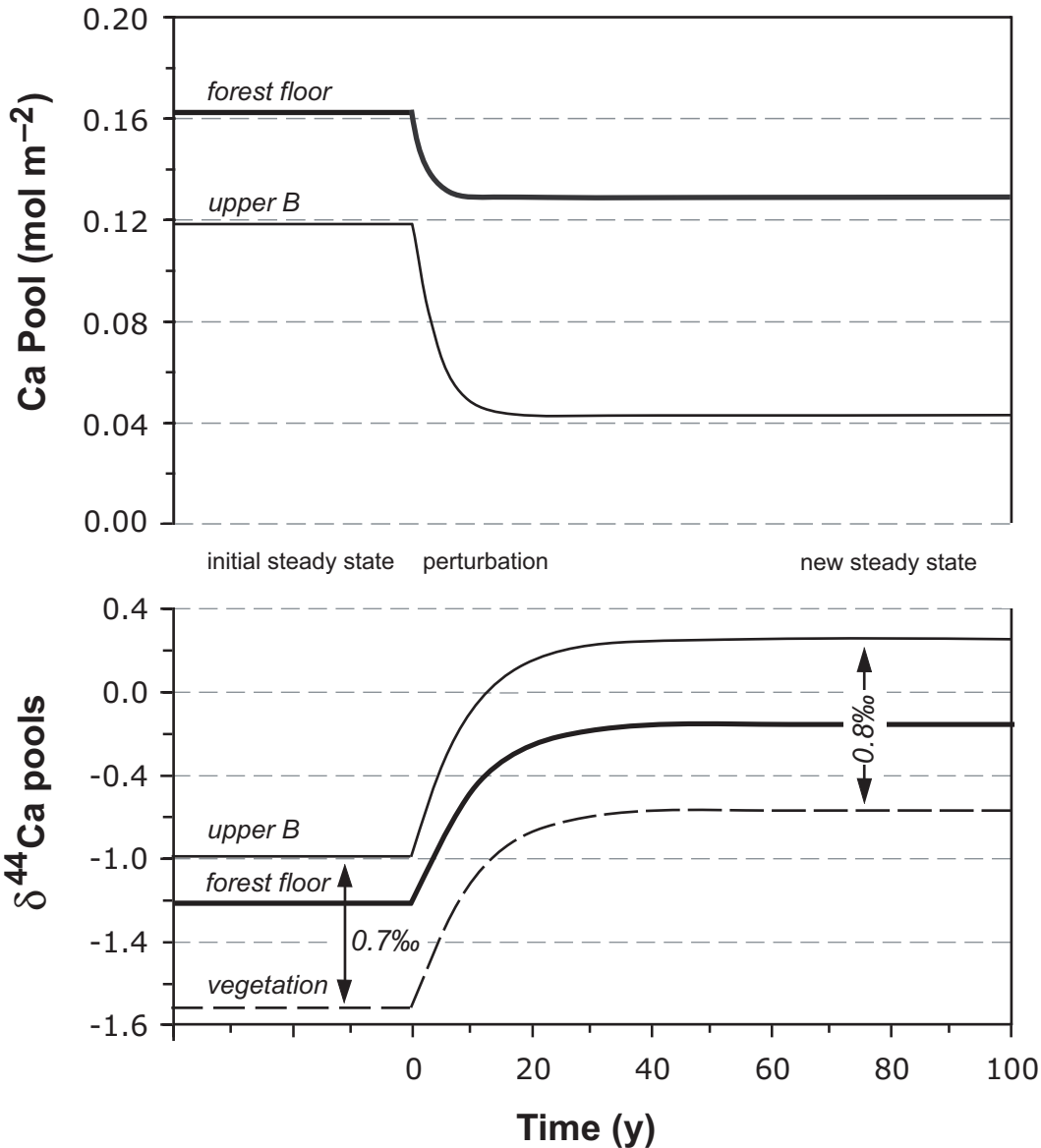
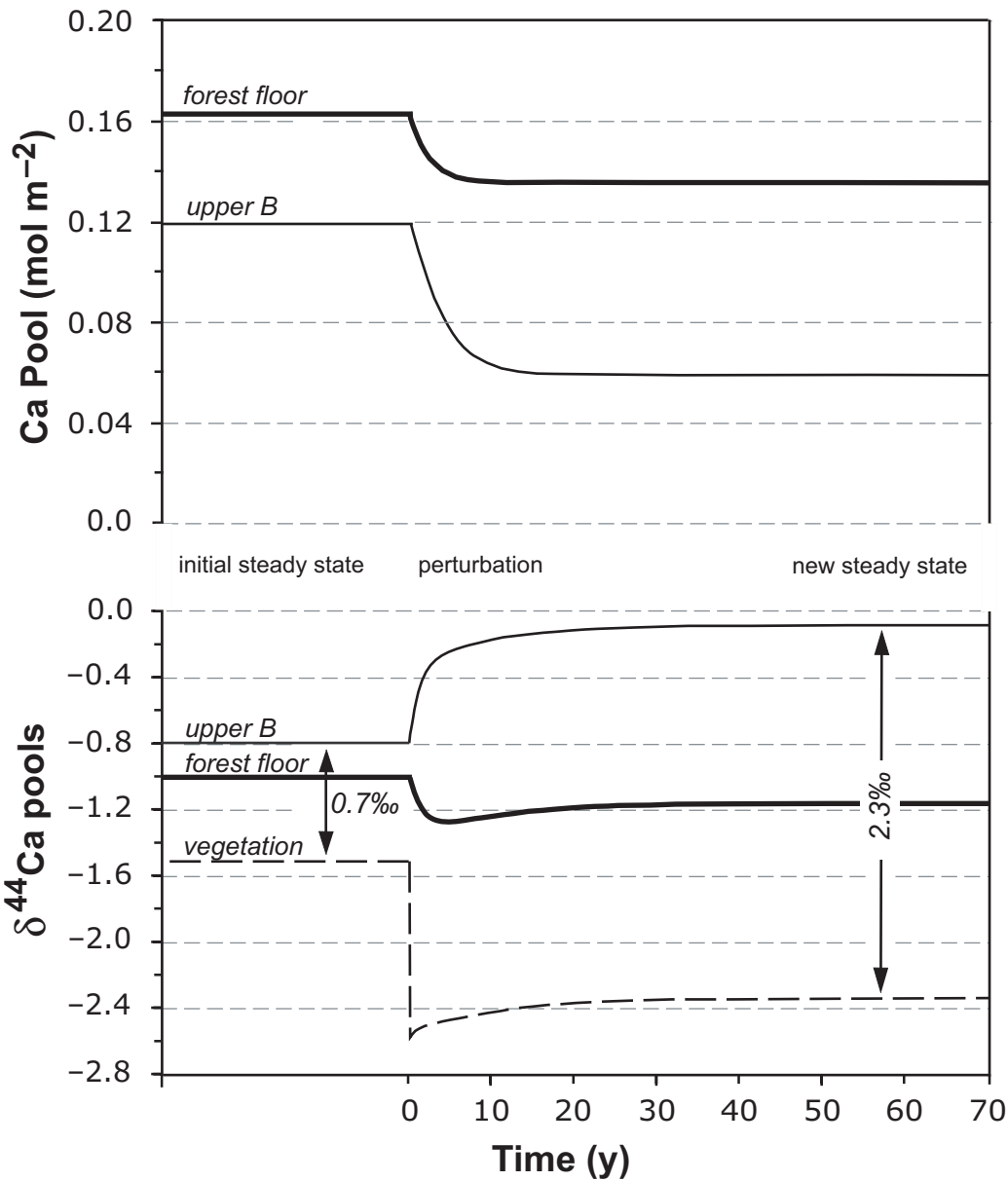


Fig. 9

Holmden and Bélanger



**Fig. 10**

Holmden and Bélanger






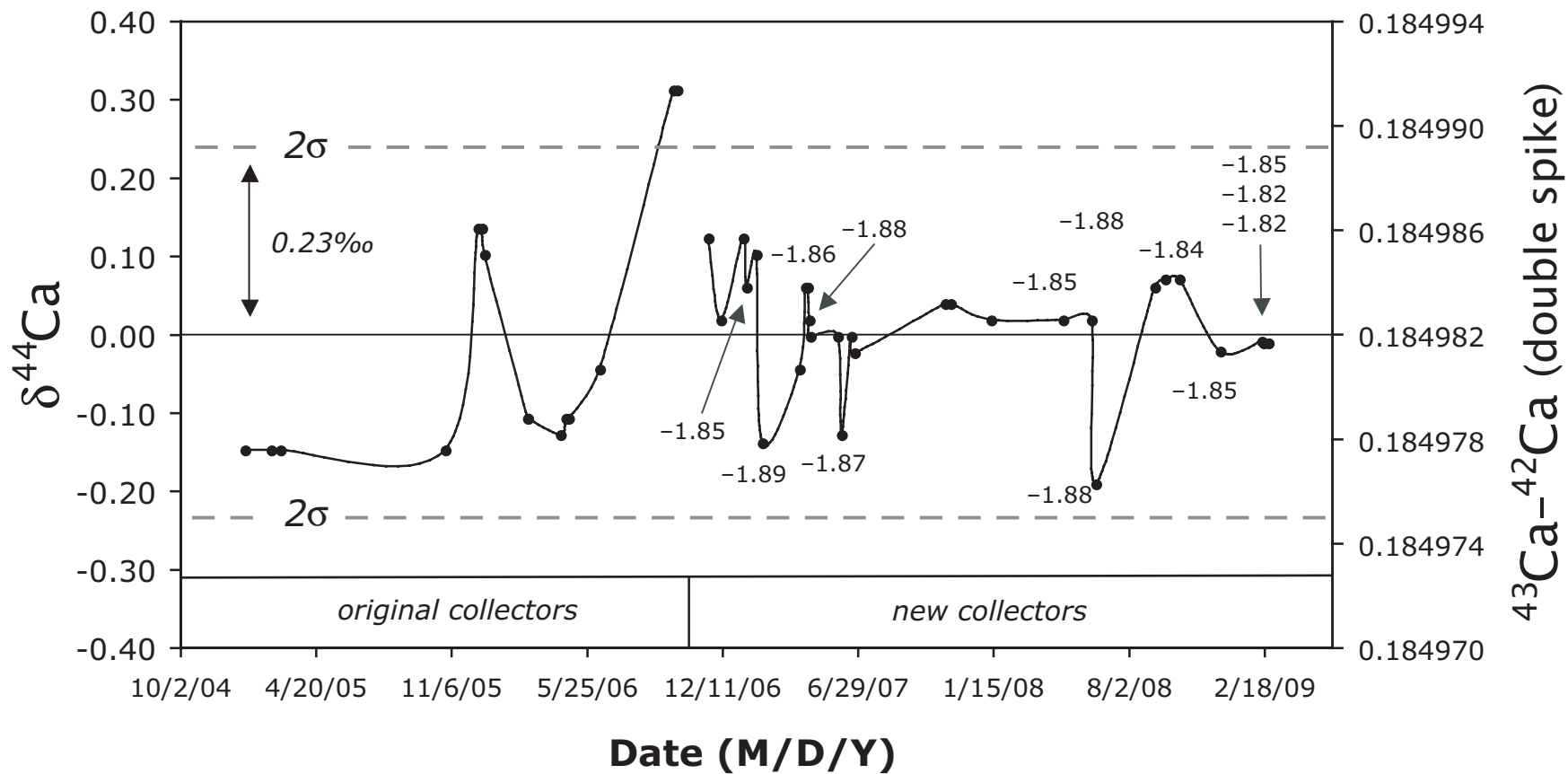
	L3	L1	Axial	H1	H3
					
Main (2s)	40		41K		42
Hop 1 (16s)		42		43	
Hop 2 (16s)		43		44	

Fig. 11

Holmden and Bélanger



**Fig. 12**

Holmden and Bélanger

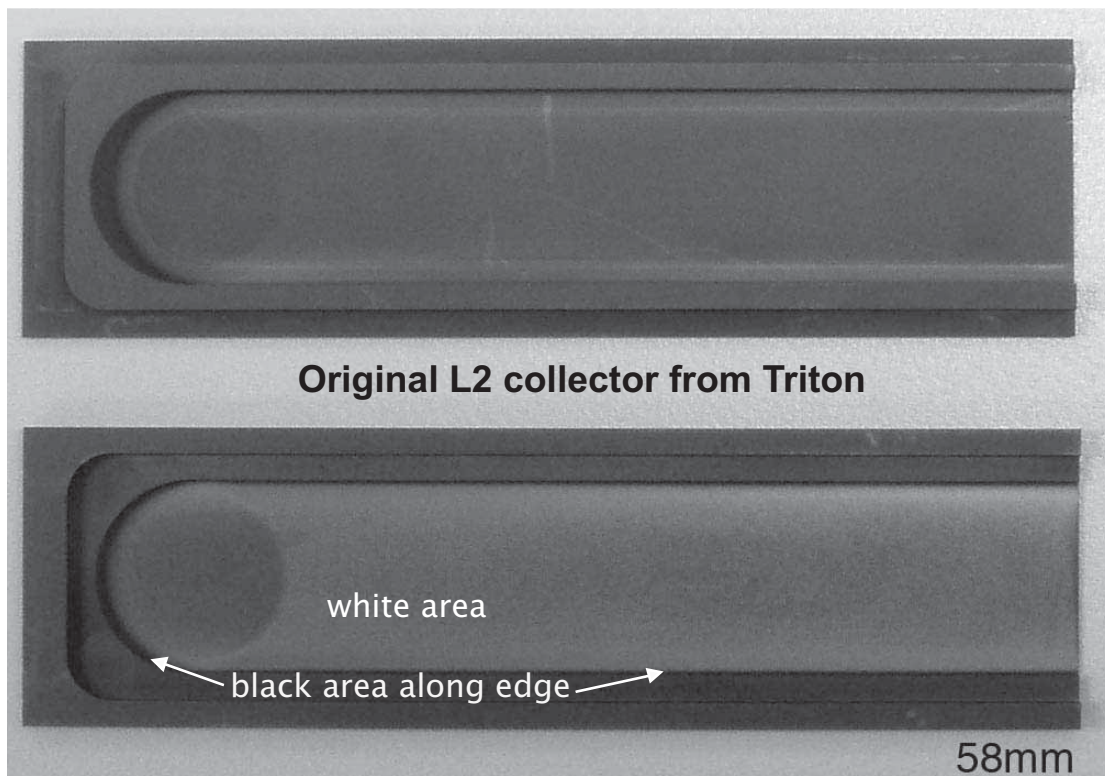


Fig. 13

